PREPARED FOR THE U.S. DEPARTMENT OF ENERGY,
UNDER CONTRACT DE-AC02-76CH03073

PPPL-3877
UC-70

PPPL-3877

Collisional Drift Waves in Stellarator Plasmas

by
J.L.V. Lewandowski

October 2003

PPPL
PRINCETON PLASMA
PHYSICS LABORATORY

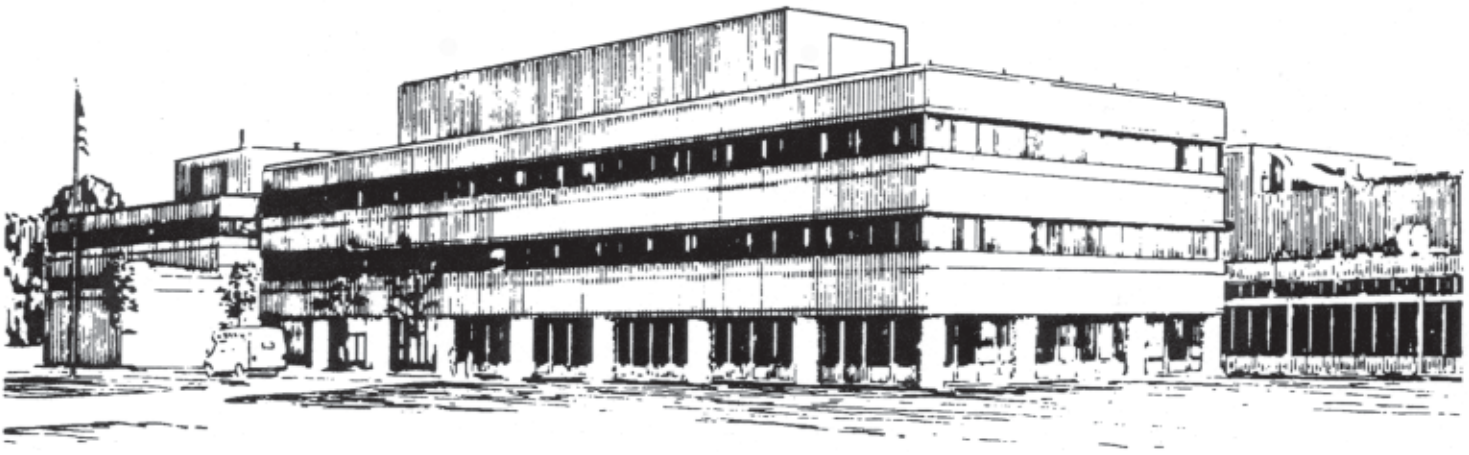

PRINCETON PLASMA PHYSICS LABORATORY
PRINCETON UNIVERSITY, PRINCETON, NEW JERSEY

PPPL Reports Disclaimer

Availability

This report is posted on the U.S. Department of Energy's Princeton Plasma Physics Laboratory Publications and Reports web site in Fiscal Year 2004. The home page for PPPL Reports and Publications is: http://www.pppl.gov/pub_report/

DOE and DOE Contractors can obtain copies of this report from:

U.S. Department of Energy
Office of Scientific and Technical Information
DOE Technical Information Services (DTIS)
P.O. Box 62
Oak Ridge, TN 37831

Telephone: (865) 576-8401

Fax: (865) 576-5728

Email: reports@adonis.osti.gov

This report is available to the general public from:

National Technical Information Service
U.S. Department of Commerce
5285 Port Royal Road
Springfield, VA 22161

Telephone: 1-800-553-6847 or
(703) 605-6000

Fax: (703) 321-8547

Internet: http://www.ntis.gov/ordering.htm

Collisional Drift Waves in Stellarator Plasmas

J. L. V. Lewandowski
Princeton University
Plasma Physics Laboratory
Princeton, P.O. Box 451, NJ 08543
USA

Abstract: A computational study of resistive drift waves in the edge plasma of a stellarator with an helical magnetic axis is presented. Three coupled field equations, describing the collisional drift wave dynamics in the linear approximation, are solved as an initial-value problem along the magnetic field line. The magnetohydrodynamic equilibrium is obtained from a three-dimensional local equilibrium model. The use of a local magnetohydrodynamic equilibrium model allows for a computationally-efficient systematic study of the impact of the magnetic field structure on drift wave stability.

Pacs: 52.35Kt, 52.30Jb, 52.35Ra

1. Introduction

There is growing evidence that slow, drift-type modes, known as drift waves, are responsible for a substantial part of the observed anomalous transport in tokamak and stellarator plasmas [1]. Drift waves represent a special class of gradient instabilities which are driven unstable by a source of free energy in the density and/or temperature gradients. In order to determine the linear properties of drift waves (and other drift-type modes satisfying $k_{||}/k_{\perp} \ll 1$, where $k_{||}$ and $k_{\perp}$ are the parallel and perpendicular wavevectors, respectively) in toroidal geometry, the model equations can be solved using the ballooning representation of Connor *et al* [2] as an eigenvalue [11] or as initial-value problem [10] for a set of representative field lines. Although some understanding of the drift wave dynamics can be gained using the so-called $i\delta$ model (for which the parameter δ is used as a tuning parameter for the drive of the instability), more realistic models usually require the solution of two or more coupled partial differential equations to be solved on a given field line. A natural approach for solving such systems of equations is to use an initial-value algorithm; this method also ensures that the fastest growing mode is (numerically) observed.

Although the topic of drift wave stability and dynamics in tokamak plasmas has been theoretically and numerically studied quite extensively, the study of low-frequency drift-type modes in stellarator geometry has received much less attention. One major reason for this state of affairs is that stellarator plasmas are inherently three-dimensional and usually require the use of sophisticated equilibrium codes to specify their magnetohydrodynamic (MHD) equilibria. As mentioned above, the most stringent linear stability considerations are usually based on the eikonal representation for perturbations; the problem is then reduced to an initial-value (or eigenvalue) problem along the magnetic field line; in general, the linear stability properties are studied one magnetic surface at a time. This observation is one motivation behind the three-dimensional local magnetohydrodynamic of Hegna [3]. Hegna's equilibrium model is particularly efficient for drift wave calculations as the MHD equilibrium is determined one surface at a time; this low-cost method allows us to study the effect of magnetic surface shaping (or parameterization) on drift wave stability. Although the initial parameterization of the magnetic surface in the local MHD equilibrium model can be quite general [see Eq.(6)], the main focus of this paper is a stellarator with an helical magnetic axis.

This paper is organized as follows; in section 2, the simplest self-consistent model equations governing resistive drift wave in a collisional plasma are presented. The characterization of the local MHD equilibrium is given in section 3. Section 4 describes the numerical method used to solve the equations governing the two-field resistive model. Numerical results are presented in section 5, and conclusions are given in section 6

2. Resistive Drift Wave Model

We consider drift waves in a low-temperature, high-density edge plasma. In a typical edge plasma, the electron-ion collision frequency can be high enough to prevent the electrons from responding instantaneously to the perturbed electrostatic potential; as a result, the nonadiabatic electron response does not vanish and the background density gradient feeds the unstable drift mode. The most unstable modes are strongly elongated along the direction of the equilibrium magnetic field $\left(k_{||}/k_{\perp} \ll 1\right)$ and it is convenient to use the eikonal representation for each fluctuating quantity $\widetilde{f}$

$$\widetilde{f} = \widehat{f}\left(\overline{\theta}, t\right) \exp\left(iN\alpha\right) \ , \tag{1}$$

where $N \gg 1$ is the toroidal mode number, $\alpha = \theta - \iota\zeta$ is the field line label, θ is the magnetic poloidal angle, ζ is the magnetic toroidal angle, ι is the rotational transform. Here $\widehat{f}\left(\overline{\theta}, t\right)$ is the amplitude which varies slowly with the extended poloidal angle, $\overline{\theta}$.

In a low-β, cold-ion plasma , the model equations governing resistive drift wave (see Appendix A

for details) are: the quasineutrality equation

$$\frac{1}{\overline{B}^2}\,\frac{\partial \overline{\omega}}{\partial \overline{t}} \;= 2\xi \overline{B} L_n \nabla_{||}\left(\frac{L_n}{\overline{B}}\,\nabla_{||}\widetilde{g}\right) - 2\mathbf{Q}\cdot\frac{\widehat{\mathbf{b}}\times\rho_{s0}\boldsymbol{\nabla}\left(\widetilde{n}\;+\widetilde{T}_e\right)}{\overline{B}}\;, \tag{2}$$

the electron continuity equation

$$\frac{\partial \widetilde{n}}{\partial \overline{t}} \;= \boldsymbol{\nabla}\rho\cdot\frac{\widehat{\mathbf{b}}\times\rho_{s0}\boldsymbol{\nabla}\widetilde{\Phi}}{\overline{B}} \;- 2\mathbf{Q}\cdot\frac{\widehat{\mathbf{b}}\times\rho_{s0}\boldsymbol{\nabla}\left(\widetilde{h}\;+\widetilde{T}_e\right)}{\overline{B}} \;+ 2\xi\overline{B}L_n\nabla_{||}\left(\frac{L_n}{\overline{B}}\,\nabla_{||}\widetilde{g}\right)\;, \tag{3}$$

and the electron energy equation

$$\frac{\partial \widetilde{T}_e}{\partial \overline{t}} \;= \eta_e\boldsymbol{\nabla}\rho\cdot\frac{\widehat{\mathbf{b}}\times\rho_{s0}\boldsymbol{\nabla}\widetilde{\Phi}}{\overline{B}} \;+ 2\xi\overline{B}L_n\nabla_{||}\left(\frac{L_n\nabla_{||}\widetilde{\varphi}}{\overline{B}}\right) - \frac{4}{3}\,\mathbf{Q}\cdot\frac{\widehat{\mathbf{b}}\times\rho_{s0}\boldsymbol{\nabla}\widetilde{\psi}}{\overline{B}}\;, \tag{4}$$

where $\overline{\omega} = {\rho_{s0}}^2\nabla_\perp^2\widetilde{\Phi}$ and $\xi \equiv \omega_\star\tau_e\,(m_i/m_e) \gg 1$ is termed the collisional parameter; $\omega_\star = \sqrt{T_e/m_i}/L_n$ is the drift frequency, L_n is the density scalelength, $\mathbf{Q} \equiv L_n\boldsymbol{\nabla}B/B$ is related to the curvature of the magnetic field and $\rho_{s0} = \sqrt{T_e/m_i}/\left(eB_0/m_ic\right)$; $\overline{B} \equiv B/B_0$ where B_0 is a magnetic field of reference (see next section); $\widetilde{g} = \widetilde{h} + (1+c_1)\widetilde{T}_e$, $\widetilde{\varphi} = \frac{2}{3}\,(1+c_1)\widetilde{g} + \frac{c_2}{3}\,\widetilde{T}_e$, $\widetilde{\psi} = \widetilde{h} + \frac{7}{2}\,\widetilde{T}_e$ and $\widetilde{h} = \widetilde{n} - \widetilde{\Phi}$ is the nonadiabatic response of the electrons. The thermoelectric coefficients c_1 and c_2 given by Braginskii are $c_1 = 0.71$ and $c_2 = 3.2$. The normalized time is $\overline{t} = \omega_\star t$ where $\omega_\star$ is the drift frequency. Here $\rho = \rho\,(\psi)$ is a radial coordinate satisfying $\mathbf{B}\cdot\boldsymbol{\nabla}\rho = 0$ which is defined in the next section. The normalized fluctuating fields in the above equations are given by $\left(\widetilde{\Phi}, \widetilde{n}\,, \widetilde{T}_e\right) = \left(e\Phi/T_{e0}, \delta n/n_0, \delta T_e/T_{e0}\right)$, where a subscript '0' denote an equilibrium quantity. The termms involving $\mathbf{Q}$ in Eqs.(2-4) arise because the divergence of the $\mathbf{E}\times\mathbf{B}$ drift velocity and the divergence of the electron diamagnetic flux do not vanish in a sheared $\mathbf{B}$ field. The first term on the right-hand side of Eq.(3) is the free energy, contained in the background density gradient, that drives the drift wave. As it is evident in Eqs.(2,3), the key parameter is the collisional parameter, ξ, which is inversely proportional to the collision frequency: in presence of collisions, the electrons cannot achieve perfect adiabicity along the field lines and the drift mode can become unstable. In practice, Eqs.(2,3) are solved as an initial-value problem for the amplitudes $\widehat{\Phi}$, $\widehat{n}$ and $\widehat{T}_e$. The MHD equilibrium quantities that enter Eqs.(2-4) are determined in the next section.

3. Local magnetohydrodynamic equilibrium

The confining magnetic field is written in straight-field line coordinates

$$\mathbf{B} = \boldsymbol{\nabla}\psi\times\boldsymbol{\nabla}\alpha\;, \tag{5}$$

where $\alpha \equiv \theta - \iota\zeta$ is the field line label, θ is the magnetic poloidal angle, ζ is the magnetic toroidal angle, ι is the rotational transform, and ψ is related to the magnetic toroidal flux. Without loss of generality, one can specify the shape of the magnetic surface in terms of the cylindrical coordinates (R, ϕ, Z) as

$$\begin{aligned} R &= \sum_{m=0}^{M}\sum_{n=-N}^{N} R_{mn}\cos\left(\varphi_{mn}\right)\;, \\ \phi &= -\zeta + \sum_{m=0}^{M}\sum_{n=-N}^{N} \phi_{mn}\sin\left(\varphi_{mn}\right)\;, \\ Z &= \sum_{m=0}^{M}\sum_{n=-N}^{N} Z_{mn}\sin\left(\varphi_{mn}\right)\;, \end{aligned} \tag{6}$$

where $\varphi_{mn} \equiv m\theta + nN_p\zeta$, N_p is the number of field periods, and the poloidal and toroidal Fourier mode numbers M and N, as well as the amplitudes $\{R_{mn}, \phi_{mn}, Z_{mn}\}$, are free parameters. Using the parameterization (6) one can determine the covariant basis vectors $\mathbf{e}_\theta = \partial\mathbf{r}/\partial\theta$ and $\mathbf{e}_\zeta = \partial\mathbf{r}/\partial\zeta$, where $\mathbf{r}$ is the position vector, and the metric elements $g_{\theta\theta} = \mathbf{e}_\theta{\cdot}\mathbf{e}_\theta$, $g_{\theta\zeta} = \mathbf{e}_\theta{\cdot}\mathbf{e}_\zeta$ and $g_{\zeta\zeta} = \mathbf{e}_\zeta{\cdot}\mathbf{e}_\zeta$. It is convenient to define an orthonormal vector set $\left\{\widehat{\mathbf{b}}, \widehat{\mathbf{n}}, \widehat{\mathbf{g}}\right\}$ attached to the magnetic field lines

$$\begin{aligned}
\widehat{\mathbf{b}} &\equiv \frac{\mathbf{B}}{B} = \frac{\mathbf{e}_\eta}{|\mathbf{e}_\eta|} \qquad (\text{parallel}) \\
\widehat{\mathbf{n}} &\equiv \frac{\mathbf{e}_\theta{\times}\mathbf{e}_\zeta}{|\mathbf{e}_\theta{\times}\mathbf{e}_\zeta|} \qquad (\text{normal}) \\
\widehat{\mathbf{g}} &\equiv \widehat{\mathbf{b}}{\times}\widehat{\mathbf{n}} \qquad (\text{geodesic})
\end{aligned} \tag{7}$$

where $\mathbf{e}_\eta \equiv \mathbf{e}_\zeta + \iota\mathbf{e}_\theta$. The vector set $\left\{\widehat{\mathbf{b}}, \widehat{\mathbf{n}}, \widehat{\mathbf{g}}\right\}$ can be determined from the parameterization (6). Finally, one can calculate important geometrical attributes of the confining $\mathbf{B}$ field such as the geodesic curvature, $\kappa_g = \widehat{\mathbf{g}}{\cdot}[(\widehat{\mathbf{b}}{\cdot}\boldsymbol{\nabla})\widehat{\mathbf{b}}]$, the normal curvature, $\kappa_n = \widehat{\mathbf{n}}{\cdot}[(\widehat{\mathbf{b}}{\cdot}\boldsymbol{\nabla})\widehat{\mathbf{b}}]$, and the normal torsion $\tau_n = -\widehat{\mathbf{n}}{\cdot}[(\widehat{\mathbf{b}}{\cdot}\boldsymbol{\nabla})\widehat{\mathbf{g}}]$. In order to determine the Jacobian of the transformation, $\mathcal{J} = \left[\boldsymbol{\nabla}\psi{\cdot}\left(\boldsymbol{\nabla}\theta{\times}\boldsymbol{\nabla}\zeta\right)\right]^{-1} = \mathbf{e}_\psi{\cdot}\left(\mathbf{e}_\theta{\times}\mathbf{e}_\zeta\right)$, we demand that the normal current vanishes everywhere on the magnetic surface [3]; using Ampere's law, one then has $J_n \equiv \widehat{\mathbf{n}}{\cdot}\mathbf{J} \propto \boldsymbol{\nabla}\psi{\cdot}\left(\boldsymbol{\nabla}{\times}\mathbf{B}\right) \equiv 0$, or

$$\frac{\partial}{\partial\theta}\left(\frac{F\left(\theta,\zeta\right)}{\mathcal{J}}\right) = \frac{\partial}{\partial\zeta}\left(\frac{G\left(\theta,\zeta\right)}{\mathcal{J}}\right) , \tag{8}$$

where

$$\begin{aligned}
F\left(\theta,\zeta\right) &= g_{\zeta\zeta} + \iota g_{\theta\zeta} , \\
G\left(\theta,\zeta\right) &= g_{\theta\zeta} + \iota g_{\theta\theta} .
\end{aligned} \tag{9}$$

Eq.(8) introduces the primary constraint on the choice $\mathbf{r} = \mathbf{r}(\theta,\zeta)$ [Eq.(6)]. Eq.(8) is termed the Jacobian constraint. Note that in the axisymmetric case, the Jacobian constraint admits the exact solution of

$$\mathcal{J} = f\left(\psi\right) F\left(\theta,\zeta\right) , \tag{10}$$

where $f(\psi)$ is an arbitrary flux surface quantity. In the general case, Eq.(8) must be solved numerically. Assuming that a solution has been found, one can construct $\boldsymbol{\nabla}\psi = \left(\mathbf{e}_\theta{\times}\mathbf{e}_\zeta\right)/\mathcal{J}$ and $\mathbf{B} = \mathbf{e}_\eta/\mathcal{J}$. The next step consists in calcultating the parallel current density consistent with the radial force balance equation and the quasineutrality condition. Using the radial force balance equation

$$\mathbf{J}{\times}\mathbf{B} = c\boldsymbol{\nabla}p ,$$

in the quasineutrality condition, $\boldsymbol{\nabla}{\cdot}\mathbf{J} = 0$, one obtains

$$\boldsymbol{\nabla}{\cdot}\mathbf{J}_{||} = -\boldsymbol{\nabla}{\cdot}\mathbf{J}_\perp = 2c\frac{dp}{d\psi}\,\frac{|\boldsymbol{\nabla}\psi|}{B}\,\kappa_g , \tag{11}$$

where the Jacobian constraint, Eq.(8), has been used. Substituting $\sigma \equiv \mathbf{J}{\cdot}\mathbf{B}/B^2 = \langle\sigma\rangle + \widehat{\sigma}$ in Eq.(11), one arrives at the equation of

$$\mathbf{B}{\cdot}\boldsymbol{\nabla}\lambda = 2\frac{|\boldsymbol{\nabla}\psi|}{B}\,\kappa_g . \tag{12}$$

where $\lambda \equiv \widehat{\sigma}/\left(cp'\right)$ (a prime denotes a derivative with respect to the toroidal flux function) and the quantity $|\boldsymbol{\nabla}\psi|/B$ can be calculated directly from the parameterization (6)

$$\frac{|\boldsymbol{\nabla}\psi|}{B} = \sqrt{\frac{g_{\theta\theta}g_{\zeta\zeta} - {g_{\theta\zeta}}^2}{g_{\zeta\zeta} + 2\iota g_{\theta\zeta} + \iota^2 g_{\theta\theta}}} . \tag{13}$$

The flux surface quantity $\langle\sigma\rangle$ is yet to be determined. The flux surface average of any function F is defined as

$$\langle F\rangle \equiv \frac{\int_0^{2\pi} d\zeta \int_0^{2\pi} d\theta \mathcal{J} F}{\int_0^{2\pi} d\zeta \int_0^{2\pi} d\theta \mathcal{J}} = \frac{1}{V'} \int_0^{2\pi} d\zeta \int_0^{2\pi} d\theta \mathcal{J} F \ , \tag{14}$$

where V is the plasma volume enclosed within ψ. Note that if $\mathcal{J}$ is a solution of Eq.(8), then $f(\psi)\mathcal{J}$ is also a solution of the same equation. Since the arbitrary flux surface function $f(\psi)$ is not known, the quantity V' is left undetermined; in practice, V' is used as an overall normalization factor. The flux surface quantity $\langle\sigma\rangle$ can be obtained through the local magnetic shear defined as $S \equiv \widehat{\mathbf{g}}\cdot\boldsymbol{\nabla}\times\widehat{\mathbf{g}}$, which can also be written as (Appendix B)

$$S = \frac{|\boldsymbol{\nabla}\psi|^2}{B^2} \mathbf{B}\cdot\boldsymbol{\nabla} \left(D + \zeta \frac{d\iota}{d\psi} \right) \ , \tag{15}$$

where

$$D \equiv \frac{\iota \boldsymbol{\nabla}\zeta\cdot\boldsymbol{\nabla}\psi - \boldsymbol{\nabla}\theta\cdot\boldsymbol{\nabla}\psi}{\boldsymbol{\nabla}\psi\cdot\boldsymbol{\nabla}\psi} \ . \tag{16}$$

Using $\mathbf{B}\cdot\boldsymbol{\nabla}\zeta = 1/\mathcal{J}$ and noting that the flux surface average operator, $\langle\bullet\rangle$, annihilates the $\mathbf{B}\cdot\boldsymbol{\nabla}$ operator, we get from Eq.(15)

$$\left\langle \frac{SB^2}{|\boldsymbol{\nabla}\psi|^2} \right\rangle = 4\pi^2 \frac{\iota'}{V'} \ . \tag{17}$$

Substituting $S = 4\pi J_{||}/(cB) - 2\tau_n$ in the left-hand side of Eq.(17) and noting that $\langle\widehat{\sigma}\rangle \equiv 0$, one obtains

$$\langle\sigma\rangle = c\sigma_0 - c\sigma_1 \frac{dp}{d\psi} - c\sigma_2 \frac{d\iota}{d\psi} \ , \tag{18}$$

where $\sigma_0 = C_3/\left(2\pi C_1\right)$, $\sigma_1 = C_2/C_1$ and $\sigma_2 = \pi/C_1$; we have defined

$$C_1 = \int_0^{2\pi} d\zeta \int_0^{2\pi} \frac{B^2\mathcal{J}}{g^{\psi\psi}} \, d\theta \ ,$$

$$C_2 = \int_0^{2\pi} d\zeta \int_0^{2\pi} \frac{B^2\mathcal{J}\lambda}{g^{\psi\psi}} \, d\theta \ ,$$

and

$$C_3 = \int_0^{2\pi} d\zeta \int_0^{2\pi} \frac{B^2\mathcal{J}\tau_n}{g^{\psi\psi}} \, d\theta \ .$$

In summary, given the parameterization (6), one solves Eq.(8) for the Jacobian, followed by Eq.(12) for λ (which is proportional to the part of $J_{||}/B$ that varies in the magnetic surface). Given ι' and p' (free parameters) one calculates $\langle\sigma\rangle$ through Eq.(18) and the specification of the local MHD equilibrum is complete.

4. Numerical Method

In this section, the numerical method used to solve the two-field resistive drift wave model is presented. The motivation for using a semi-implicit algorithm is discussed.

The radial coordinate is conveniently defined as $\rho \equiv R_0\sqrt{2\overline{\psi}}$ where $\overline{\psi} \equiv \psi/\psi_0$ and $\psi_0 = B_0{R_0}^2$ and $R_0 \equiv R_{00}$ is the major radius [in the large-aspect ratio tokamak equilibrium, $\psi \simeq B_0 r^2/2$ where

B_0 is the magnetic field strength evaluated at the magnetic axis; it follows that $\rho = r$ in this case]. In the general 3D case, it is convenient to define a magnetic field strength of reference as $B_0 \equiv \left\langle B^2 \right\rangle^{1/2}$. Using the eikonal representation [Eq.(1)] in the quasineutrality condition [Eq.(2)], the electron continuity equation [Eq.(3)] and the electron energy equation [Eq.(4)] we obtain

$$\frac{\partial \widehat{\Phi}}{\partial \overline{t}} = -\eta D_{||} - i\eta\nu_{\perp}\left(\widehat{n} + \widehat{T}_e\right) , \tag{19}$$

$$\frac{\partial \widehat{n}}{\partial \overline{t}} = -i\sqrt{b}\widehat{\Phi} + D_{||} + i\nu_{\perp}\left(\widehat{n} - \widehat{\Phi} + \widehat{T}_e\right) , \tag{20}$$

and

$$\frac{\partial \widehat{T}_e}{\partial \overline{t}} = -i\eta_e\sqrt{b}\widehat{\Phi} + \widehat{D}_{||} + \frac{2}{3}\, i\nu_{\perp}\widehat{\psi} , \tag{21}$$

where the terms related to the transport along the field line are given by

$$D_{||} = \nu_{||}\overline{B}S_{||}\frac{\partial}{\partial \overline{\theta}}\left(\frac{S_{||}}{\overline{B}}\,\frac{\partial \widehat{g}}{\partial \overline{\theta}}\right) , \tag{22}$$

and

$$\widehat{D}_{||} = \nu_{||}\overline{B}S_{||}\frac{\partial}{\partial \overline{\theta}}\left(\frac{S_{||}}{\overline{B}}\,\frac{\partial \widehat{\varphi}}{\partial \overline{\theta}}\right) . \tag{23}$$

Here $S_{||}(\overline{\theta}) = 1/\left(\overline{\mathcal{J}B}\right)$, $\overline{\mathcal{J}} = \left[R_0\boldsymbol{\nabla}\overline{\psi}\cdot\left(R_0\boldsymbol{\nabla}\theta\times R_0\boldsymbol{\nabla}\zeta\right)\right]^{-1}$ is the dimensionless Jacobian and $\nu_{||} = 2\xi\epsilon_n^2/q^2$ is related to the parallel transport of current density. The perpendicular transport is controlled by the curvature term

$$\nu_{\perp}\left(\overline{\theta}\right) \equiv 2\sqrt{b}\,\epsilon\,\epsilon_n S_{\perp}\left(\overline{\theta}\right) , \tag{24}$$

which arises from the divergence of the electron diamagnetic flux and the divergence of the $\mathbf{E}\times\mathbf{B}$ drift velocity. In the above equations, we have defined $b \equiv \left(k_\theta\rho_{\mathrm{s0}}\right)^2$, $k_\theta \equiv N/\overline{a}$ is the characteristic perpendicular wavevector (i.e. $|\boldsymbol{\nabla}\alpha|^2_{\overline{\theta}=0} \sim k_\theta^2$), $\epsilon_n \equiv L_n/R_0$ and $\epsilon \equiv \overline{a}/R_0$ is the inverse aspect ratio. The geometrical quantities $\mathcal{L}$ and $S_\perp$ are defined as

$$\mathcal{L}\left(\overline{\theta}\right) \equiv \frac{1+\Lambda^2}{R_0^2 g^{\overline{\psi\psi}}} , \tag{25}$$

$$S_{\perp}\left(\overline{\theta}\right) \equiv \frac{\kappa_n + \Lambda\kappa_g}{\sqrt{g^{\overline{\psi\psi}}}} , \tag{26}$$

and

$$\Lambda\left(\overline{\theta}\right) \equiv -\frac{\boldsymbol{\nabla}\psi\cdot\boldsymbol{\nabla}\alpha}{B} . \tag{27}$$

Finally $\eta\left(\overline{\theta}\right) \equiv 1/\left(b\epsilon^2\mathcal{L}\right) \simeq 1/\overline{\theta}^2$ for large $\left|\overline{\theta}\right|$. In view of the secular behavior of the polarization term ($\mathcal{L} \sim \overline{\theta}^2$ for $\left|\overline{\theta}\right| \gg 1$), it is numerically convenient to solve for the nonadiabatic response $\widehat{h} \equiv \widehat{n} - \widehat{\Phi}$ instead of solving the quasineutrality equation (19). The system of equations to be solved can then be written as

$$\frac{\partial \widehat{n}}{\partial \overline{t}} = -i\sqrt{b}\widehat{\Phi} + D_{||} + i\nu_{\perp}\left(\widehat{h} + \widehat{T}_e\right) , \tag{28}$$

$$\frac{\partial \widehat{h}}{\partial \overline{t}} = -i\sqrt{b}\widehat{\Phi} + (1+\eta)D_{||} + i\nu_{\perp}\widehat{h} + i\nu_{\perp}\left[\eta\widehat{n} + (1+\eta)\,\widehat{T}_e\right] \ , \tag{29}$$

and

$$\frac{\partial \widehat{T}_e}{\partial \overline{t}} = -i\eta_e\sqrt{b}\widehat{\Phi} + \widehat{D}_{||} + \frac{2}{3}\,i\nu_{\perp}\widehat{\psi} \, . \tag{30}$$

Eqs.(28-30) are discretized on the domain $\overline{\theta} \in \left[-\overline{\theta}_{\max}, +\overline{\theta}_{\max}\right]$ where $\overline{\theta}_{\max}$ is a free parameter. In a low-temperature, high-density edge plasma the collisional parameter is much larger than unity [typically $\xi = \mathcal{O}\left(10^2\right)$] and one expects the parallel transport to be strong. Therefore a numerical method based on an explicit scheme will require a very small time step. The time step for an explicit method is constrained by the transport along the magnetic field lines and must be less than the well-known Courant-Friedrichs-Lewy (CFL) criterion [4] of

$$\Delta t < (\Delta t)_{\mathrm{CFL}} \equiv \frac{q^2\left(\Delta\overline{\theta}\right)^2}{2\xi{\epsilon_n}^2} \ , \tag{31}$$

where $\Delta\overline{\theta}$ is the grid spacing. In practise, the grid spacing $\Delta\overline{\theta}$ must be chosen small enough as to capture the details of the equilibrium along the magnetic field line. In order to bypass the stringent condition (31) we must resort to an implicit scheme. As it turns out, for the system of Eqs.(28-30), it is sufficient to use a semi-implicit numerical scheme; this is done by treating $\partial\widehat{n}/\partial\overline{t}$, $\partial\widehat{h}/\partial\overline{t}$ and $\partial\widehat{T}_e/\partial\overline{t}$ and the parallel transport terms [terms in $D_{||}$ and $\widehat{D}_{||}$ in Eq.(28-30)] implicitly whereas the remaining terms are treated explicitly. As a result one obtains a set of coupled tridiagonal systems which can be solved sequentially using standard algorithms, such as the Thomas algorithm [9].

Since the system of equations (19-21) is solved as an initial-value problem, the linear growth rate and the mode frequency must be computed dynamically. Another consequence associated with the initial value approach is that only the fastest growing mode is observed. Earlier studies [5, 6] of drift wave stability in realistic stellarator equilibria have shown that the drift wave spectrum can have a rather complicated structure; in some cases, it can be difficult to 'pick up' the most unstable mode.

In order to determine the mode frequency, we use the transformation of

$$\widehat{f}\left(\overline{\theta}, t\right) \mapsto \overline{f}\left(\overline{\theta}\right)\exp\left(-i\omega_f t\right) \ .$$

where $\widehat{f}$ stands for $\widehat{\Phi}, \widehat{n}$ or $\widehat{T}_e$. Since the intial conditions are arbitrary, it is very likely that the initial profiles for $\widehat{\Phi}, \widehat{n}$ and $\widehat{T}_e$ will *not* correspond to the most unstable eigenfunctions. In other words, the scalar fields $\widehat{\Phi}, \widehat{n}$ and $\widehat{T}_e$ will possess different frequencies ω_f. Once the transitory effects have disappeared, we expect $\omega_\Phi = \omega_n = \omega_{T_e} \equiv \omega$.

The normal mode frequency can be written as $\omega_f = \Re\left(\omega_f\right) + i\Im\left(\omega_f\right) \equiv \omega_{\mathrm{r}f} + i\gamma_f$. Noting that

$$\frac{\partial \widehat{f}}{\partial t} = \frac{1}{2}\,\frac{1}{\left|\widehat{f}\right|}\,\frac{\partial}{\partial t}\,\left|\widehat{f}\right|^2 - i\omega_{\mathrm{r}f}\left|\widehat{f}\right| \ ,$$

we obtain

$$\gamma_f = \frac{1}{\left|\left\langle\widehat{f}\right\rangle_{\overline{\theta}}\right|}\,\frac{\partial}{\partial t}\,\left|\left\langle\widehat{f}\right\rangle_{\overline{\theta}}\right| \ , \tag{32}$$

for the linear growth rate and

$$\omega_{\mathrm{r}f} = -\Im\left(\frac{1}{\left\langle\widehat{f}\right\rangle_{\overline{\theta}}}\,\frac{\partial}{\partial t}\,\left\langle\widehat{f}\right\rangle_{\overline{\theta}}\right) \ , \tag{33}$$

for the mode frequency. In the above equations, we have defined the field-line average operator as

$$\langle F\rangle_{\overline{\theta}} \equiv \frac{1}{2\overline{\theta}_{\max}} \int_{-\overline{\theta}_{\max}}^{+\overline{\theta}_{\max}} F\left(\overline{\theta}^{'}, t\right) d\overline{\theta}^{'} \ , \tag{34}$$

for any function $F\left(\overline{\theta}, t\right)$. The free parameter in Eq.(34) must be large enough so that the linear growth rate [Eq.(32)] and the mode frequency [Eq.(33)] become independent of $\overline{\theta}_{\max}$; a convergence study using this parameter is presented in the next section. In practise, it is convenient to define an average linear growth, $\gamma = \left(\gamma_\Phi + \gamma_n + \gamma_{T_e}\right)/3$, and an average mode frequency, $\omega_{\rm r} = \left(\omega_{{\rm r}\Phi} + \omega_{{\rm r}n} + \omega_{{\rm r}T_e}\right)/3$.

5. Numerical Results

As described in section 3, the specification of the local MHD equilibrium depends on 2 free parameters, ι' and p'. It is convenient to use normalized quantities instead of ι' and p'; to make the connection with the standard large-aspect ratio tokamak notation, we define the ballooning parameter

$$\alpha_b \equiv \frac{2}{\pi^2 \iota^2} \frac{V'}{\left\langle \frac{B^2}{g^{\psi\psi}} \right\rangle^{1/2}} \ , \tag{35}$$

and the global shear parameter

$$s_b \equiv -\frac{4\pi^2 R_0}{V'} \frac{\frac{1}{\iota}\frac{d\iota}{d\psi}}{\left\langle \frac{B^2}{g^{\psi\psi}} \right\rangle} \ . \tag{36}$$

As mentioned in the Introduction, the initial parameterization of the magnetic surface [Eq.(6)] is quite general. However, in order to illustrate the usefulness and efficiency of the local equilibrium model for drift wave stability calculations, we consider the parameterization of

$$\begin{aligned} R &= R_0\left[1 + \epsilon_{\rm t}\cos\theta + \epsilon_{\rm h}\cos\left(N_p\zeta\right)\right] \ , \\ \phi &= -\zeta \ , \\ Z &= R_0\left[\epsilon_{\rm t}\sin\theta + \epsilon_{\rm h}\sin\left(N_p\zeta\right)\right] \ , \end{aligned} \tag{37}$$

where, as before, N_p is the number of field periods; $\epsilon_{\rm t}$ and $\epsilon_{\rm h}$ are termed the toroidicity parameter and the helical parameter, respectively. In the remaining of this paper, we refer to Eq.(37) as the helical parameterization. Note that the case $\epsilon_{\rm h} = 0$ in Eq.(37) corresponds to the tokamak parameterization with concentric, circular magnetic surfaces (which is valid for a low-β plasma). When the parameter $\epsilon \equiv N_p^2 \epsilon_{\rm t}\epsilon_{\rm h}$ is less than unity, the Jacobian for the helical parameterization can be calculated analytically (Appendix C)

$$\mathcal{J} = \frac{X^2\left(\theta\right)}{A_0\left(\psi\right) g\left(\varphi\right)} \ , \tag{38}$$

where $\varphi \equiv N_p\zeta - \theta$ is the helical coordinate, $A_0(\psi)$ is an arbitrary flux function, $X(\theta) = R_0\left(1 + \epsilon_{\rm t}\cos\theta\right)$ and

$$g\left(\varphi\right) = 1 + a\left(1 - \cos\varphi\right) - b\sin^2\varphi \ . \tag{39}$$

Here $a = \xi(1 + \xi/\widehat{\alpha})/\widehat{\alpha}$, $b = \xi(\widehat{\beta} + \xi)/(2\widehat{\alpha}^2)$, $\widehat{\alpha} = 1 + {\epsilon_{\rm t}}^2\left(N_p\iota + \frac{1}{2}\right) + {\epsilon_{\rm h}}^2\left(N_p^2 + \frac{1}{2}\right)$, $\widehat{\beta} = \widehat{\epsilon}\left[1 + N_p\left(N_p + \iota\right)\right]$ and $\xi = \left[N_p\left(N_p + \iota\right) - 1\right]\epsilon_{\rm t}\epsilon_{\rm h}$. Note that for the case of the tokamak parameterization ($\epsilon_{\rm h} = 0$) we have $a = b = \xi = 0$ so that $g(\varphi) = 1$ and Eq.(38) then reduces to the exact solution of

$$\mathcal{J} = C\left(1 + \epsilon_{\rm t}\cos\theta\right)^2 \ ,$$

where C is an arbitrary multiplicative constant. When the parameter ϵ is comparable to unity, one must resort to the numerical solution described at the end of section 3.

In all simulations reported in this paper, the initial profile for $\widehat{\Phi}$ has been chosen to be a Gaussian profile with its maxima centered at $\overline{\theta} = 0$. The density profile at $t = 0$ is chosen as $\widehat{n} = \widehat{\Phi}$, that is the nonadiabatic response vanishes at $t = 0$; the electron temperature perturbation is set to zero; as a result, the parallel transport terms in Eqs.(28,29), which involve $D_{||}$, vanish at the beginning of the simulations. Since the cross-field terms in Eqs.(28,29) are not equal (even when $\widehat{n} = \widehat{\Phi}$), the non-adiabatic response becomes nonzero as time progresses. As the instability develops, the parallel transport increases in order to balance the cross-field transport; at this stage, the linear growth rate becomes almost independent of time (Figure 7).

The real (plain) and imaginary (dotted) parts of the normalized electrostatic potential amplitude at saturation ($\omega_\star t = 250$) is shown in Figure 2. The parameters are: $\alpha_b = 0$ (ballooning parameter), $s_b = 0.25$ (global shear parameter), $q = 1.03$ (safety factor), $n_0 = 5 \times 10^{12}$ cm^{-3} (equilibrium plasma density), $T_e = 5$ eV (equilibrium electron temperature), $\eta_e = 1.0$ (electron temperature gradient parameter), $k_\theta \rho_{\rm s0} = 0.8$, $B_0 = 10^4$ Gauss (equilibrium magnetic field of reference), $\Delta\overline{\theta} = \pi/128$ (grid spacing), $L_n = 4.0$ cm (density scalelength), $R_0 = 10^2$cm (major radius), $\epsilon_{\rm t} = 0.1$ (toroidicity parameter) and $\epsilon_{\rm h} = 0.04$ (helical parameter). The number of field periods is $N_p = 3$. As mentioned in section 2, the key parameter is the collisional parameter, ξ; in the low-temperature, high-density edge plasmas, this parameter can be quite large. For example, for the parameters of Figure 2, one finds $\xi \simeq 72$. Note that the most unstable eigenfunction for Φ shown in Figure 2 satisfies the proper boundary conditions at large $|\overline{\theta}|$; clearly the mode is square integrable since

$$\int_{-\infty}^{+\infty} |\widehat{\Phi}|^2 d\overline{\theta} < \infty \ .$$

Figure 3 and Figure 4 show the corresponding profile for the perturbed density amplitude and the perturbed electron temperature amplitude, respectively. We note that the fluctuating electrostatic potential and the plasma density are out of phase and that their respective amplitudes are not equal indicating that the drift mode is unstable. Note that the inclusion of perturbations in the electron temperature, $\delta T_{\rm e}$, makes the mode less unstable.

Figure 5 shows the instantaneous average real mode frequency as a function of the normalized time $\overline{t} = \omega_\star t$. The parameters are the same as those of Figures 2-4. The large $\omega_{\rm r}$ observed in the initial development of the instability is associated with the evolution of the electron temperature. After transitory effects have disappeared, the average real mode frequency reaches its steady state value.

Fgiure 6 shows the average linear growth rate as a function of the normalized time $\overline{t} = \omega_\star t$ for the same case as Figure 5. The components of the average linear growth rate of Figure 6 are shown in Figure 7. The instateneous linear growth for the electrostatic potential, plasma density and electron temperature perturbation are shown by plain, dotted and dashed lines, respectively. As expected, the profiles for γ_n and γ_{T_e} tend to be strongly coupled. Note that the initial spike in Figure 6 can be traced back to γ_{T_e} (Figure 7).

As discussed in the previous section, the field-line averaged profiles $\left\langle \widehat{f} \right\rangle_{\overline{\theta}}$ for $\widehat{f} = \left(\widehat{\Phi}, \widehat{n}, \widehat{T}_e\right)$ depend implictly on the parameter $\overline{\theta}_{\rm max}$. Therefore one must ensure that the parameter $\overline{\theta}_{\rm max}$ is large enough so that the linear growth rate and the mode frequency become independent of its value. Figures 8 and 9 show the average real mode frequency and the average linear growth rate as a function of the parameter $\overline{\theta}_{\rm max}$, respectively. Other parameters are the same as in Figures 2-7. For $\overline{\theta}_{\rm max} > 16$, the linear growth rate reaches its asymptotic value. Note that in practice the parameter $\overline{\theta}_{\rm max}$ must be increased as the global shear parameter, s_b, is decreased (the extent of the mode along the field line increases with decreasing global shear).

One advantage of the local equilibrium model is that one can modify the MHD equilibrum dynamically for a very low computational cost. This is illustrated in Figure 10 and Figure 11 for a $N_p = 3$ field

period stellarator. In these figures, the helical parameter $\epsilon_{\rm h}$, which is related to the helical excursion of the magnetic axis, has been varied while the toroidicity parameter has been kept fixed at $\epsilon_{\rm t} = 0.1$. Other parameters are the same as in Figure 2-4. As mentioned in the beginning of this section, the case $\epsilon_{\rm h} = 0$ corresponds to the tokamak parameterization (with circular magnetic surfaces). The real mode frequency (Figure 10) decreases with increasing $\epsilon_{\rm h}$ until the toroidicity parameter becomes comparable to the helical parameter. Note that for $\epsilon_{\rm t} \sim \epsilon_{\rm h}$, the helical component of the curvature dominates over its toroidal component. The average linear growth rate (Figure 11) tends to increase with an increase of the helical excursion of the magnetic axis. Note that each square in Figures 10 and 11 corresponds to a different magnetic configuration; it takes about 55 seconds on a workstation to compute the MHD equilibrium *and* the linear growth rate. If one uses a global equilibrum code, one would have to recalculate the MHD equilibrium for the *entire* plasma volume for each data point in Figs. (10,11): the use of the local equilibrium model represents an enormous reduction in the overall computational effort.

In order to understand the dependence of the linear growth rate on the helical parameter, one can compare the key attributes of the magnetic configuration for specific sets $(\epsilon_{\rm t}, \epsilon_{\rm h})$; such key attributes are the normal and geodesic components of the magnetic curvature (κ_n and κ_g, respectively), the magnetic shear, S, and the normal torsion, τ_n. Other quantities that characterize the equilibrium configuration do enter the drift wave stability calculations; however, the impact of these quantities are subdominant. The normal magnetic curvature and the magnetic shear are probably the most important quantities that affect drift wave (and ballooning) stability [5]. Figure 12 shows the normal curvature (plain line) and the local magnetic shear (dotted line) along the field line for the case of $(\epsilon_{\rm t}, \epsilon_{\rm h}) = (0.1, 0.0)$. The ballooning parameter is $\alpha_b = 0$ and the global shear parameter is $s_b = 0.25$. For these parameters, the modes are nonzero in the range $\left|\overline{\theta}\right| \lesssim 15$ (See Figs. 2-4). Figure 12 shows that the normal curvature is destabilizing (negative) in the outboard side of the torus. The magnetic shear is positive around $\overline{\theta} = 0$ but becomes negative further away along the field line. The normal curvature (plain line) and the local magnetic shear (dotted line) along the field line for the case of $(\epsilon_{\rm t}, \epsilon_{\rm h}) = (0.1, 0.1)$ is shown in Figure 13. The normal curvature has a more destabilizing influence on the drift modes as compared to Figure 13; this is one indication that the linear growth rate for the parameters of Figure 13 should be larger than for the case of Figure 12. However, one must also consider the impact of the local magnetic shear. Note that in the case of Figure 13 the bulk of the drift mode amplitude experiences a positive global shear away from the $\overline{\theta} = 0$; therefore, we expect the linear growth rate to be larger for the case of Figure 13 as compared to the case of Figure 12. The detrimental influence of a large, positive local magnetic shear on drift wave stability in realistic 3D stellararator geometries has been noted by Nadeem and coworkers [11]; these authors also discuss the case of large, negative local magnetic shear which appears to have a stabilizing influence on the drift mode. This is in agreement with our observations, although our model MHD equilibrium is far simpler than the fully 3D stellarator equilibrium used in the work of Nadeem *et al*.

Finally, another attractive feature of the local MHD equilibrium model is that it allows for fast, computationally-efficient estimates of the anomalous diffusion coefficient, $D_\perp$; such estimates, however, have to be used with caution. Based on mixing length arguments [1], one can estimate the perpendicular diffusion coefficient using the relation of

$$D_\perp \simeq D_\perp^{(\rm m)} \equiv \frac{\gamma}{k_r^2} \ , \tag{40}$$

where γ is the linear growth rate and k_r is the magnitude of a typical radial wavevector. Using a general non-Markovian Fokker-Planck treatment, Zagorodny and Weiland [8] showed that memory effects can be important for the description of transport under saturared turbulence; they derived an estimate for the perpendicular diffusion coefficient of the form

$$D_\perp \simeq D_\perp^{(\rm fp)} \equiv \frac{\gamma^3/k_r^2}{{\omega_{\rm r}}^2 + \gamma^2} = \frac{1}{1 + \left(\omega_{\rm r}/\gamma\right)^2} \, D_\perp^{(\rm m)} \ . \tag{41}$$

We note that $D_\perp^{(\mathrm{fp})} \mapsto D_\perp^{(\mathrm{m})}$ when $\gamma \gg \omega_\mathrm{r}$. An estimate for k_r in Eqs.(40,41) can be obtained by a suitable average (weighted with the eigenfunction) of the normal component of $\boldsymbol{\nabla}\alpha \propto \mathbf{k}_\perp$

$$k_r^2 = \frac{\int_{-\infty}^{+\infty} \left(\mathbf{k}_\perp \cdot \widehat{\mathbf{n}}\right)^2 |\widehat{\Phi}|^2 d\overline{\theta}}{\int_{-\infty}^{+\infty} |\widehat{\Phi}|^2 d\overline{\theta}} \ , \tag{42}$$

where

$$\mathbf{k}_\perp \cdot \widehat{\mathbf{n}} = -\frac{NB}{\sqrt{g^{\psi\psi}}}\, \Lambda(\overline{\theta}) \ .$$

Here $\Lambda(\overline{\theta})$, defined in Eq.(27), is related to the integrated local magnetic shear. Figure 14 shows the estimates for $D_\perp$ based on the mixing length theory (squares) and the non-Markovian Fokker-Planck theory (triangles). The most striking feature is that $D_\perp^{(\mathrm{fp})}$ remains almost independent of the helical parameter for moderate ϵ_h; the mixing length-based diffusion coefficient, however, shows a clear upward trend with increasing ϵ_h. Therefore, although the linear growth rate does increase with an increase in the helical parameter, the non-Markovian Fokker-Planck diffusion coefficient does not predict a substantial decrease in the confinement time. More work is needed to resolve this issue especially when effects such as plasma shaping are taken into account.

6. Conclusions

Drift wave stability calculations in stellarator geometry usually requires the use of sophisticated, computationally-intensive 3D MHD equilibrium codes. However, as far as linear stability is concerned, the general approach is to study the local drift wave stability using the ballooning representation, one magnetic surface at a time. Hegna's local equilibrium model [3] is specific to a particular magnetic surface and it is computationally very efficient.

The local equilibrium model has been used to study the drift wave stability properties of a three-field resistive model valid in the low-temperature, high-density edge plasmas of tokamaks and stellarators. It has been shown that in the case of a stellarator with a helical axis a large, positive magnetic shear can increase the linear growth rate, whereas a large, negative magnetic shear has a stabilizing influence on the drift modes.

Appendix: Derivation of the Resistive Drift Wave Model

In the cold ion limit, the ion momentum equation reads

$$m_i n \left(\frac{\partial}{\partial t} + \mathbf{V}_i \cdot \boldsymbol{\nabla} \right) \mathbf{V}_i = en \left(\mathbf{E} + \frac{\mathbf{V}_i \times \mathbf{B}}{c} \right) - \mathbf{R}_{ei} \ , \tag{A.1}$$

where $\mathbf{R}_{ei} = en \left(\mathbf{J}_{||}/\sigma_{||} + \mathbf{J}_{\perp}/\sigma_{\perp} \right) - c_1 n \nabla_{||} T_e - \frac{3}{2} \, n \widehat{\mathbf{b}} \times \boldsymbol{\nabla}_{\perp} T_e / \left(\omega_{ce} \tau_e \right)$ is the momentum transfer due to collisions; $\sigma_{||} \simeq 2\sigma_{\perp}$, $\sigma_{\perp} = e^2 n \tau_e / m_e$ are the parallel and perpendicular electron conductivities, respectively; $\tau_e = (3\sqrt{m_e} T_e^{3/2})/(4\sqrt{2\pi} n \lambda e^4)$ is the electron collision time; and $c_1 = 0.71$ is a thermoelectric coefficient. The electron momentum equation (for massless electrons) is

$$\boldsymbol{\nabla} p_e + en \left(\mathbf{E} + \frac{\mathbf{V}_e \times \mathbf{B}}{c} \right) = \mathbf{R}_{ei} \ . \tag{A.2}$$

Operating with $\mathbf{B}\times$ on Eqs.(A.1,A.2) we obtain (in the low-frequency regime of $\omega/\omega_{ci} \ll 1$)

$$\mathbf{V}_{i\perp} = \mathbf{V}_E + \mathbf{V}_{pi} + \mathbf{V}_c \ , \tag{A.3}$$

and

$$\mathbf{V}_{e\perp} = \mathbf{V}_E + \mathbf{V}_{\star e} + \mathbf{V}_c \ , \tag{A.4}$$

respectively. Here

$$\begin{aligned} \mathbf{V}_E &= \frac{c}{B^2} \, \mathbf{B} \times \boldsymbol{\nabla} \Phi \ , \\ \mathbf{V}_{pi} &= \omega_{ci}^{-1} \widehat{\mathbf{b}} \times \left(\frac{\partial}{\partial t} + \mathbf{V}_E \cdot \boldsymbol{\nabla} \right) \mathbf{V}_E \ , \\ \mathbf{V}_c &= \frac{c}{enB^2} \, \mathbf{B} \times \mathbf{R}_{ei} \ , \\ \mathbf{V}_{\star e} &= -\frac{c}{enB^2} \, \mathbf{B} \times \boldsymbol{\nabla} p_e \ , \end{aligned} \tag{A.5}$$

are the $\mathbf{E}\times\mathbf{B}$ drift velocity (in the low-β approximation of $\mathbf{E} \simeq -\boldsymbol{\nabla}\Phi$), the ion polarization drift velocity, the collisional drift velocity and the electron diamagnetic drift velocity, respectively. For low-frequency, long-wavelength modes $\left(k_{\perp}^2 \lambda_D^2 \ll 1 \right)$ (where $k_{\perp}$ is the magnitude of the perpendicular wavevector and λ_D is the Debye length), the plasma is quasineutral

$$\boldsymbol{\nabla} \cdot \mathbf{J} = 0 \ ,$$

or

$$\boldsymbol{\nabla} \cdot \mathbf{J}_{\perp} = -\mathbf{B} \cdot \boldsymbol{\nabla} \left(\frac{J_{||}}{B} \right) \ , \tag{A.6}$$

where the perpendicular current density is obtained from Eqs.(A.3,A.4)

$$\mathbf{J}_{\perp} = en \left(\mathbf{V}_{pi} - \mathbf{V}_{\star e} \right) \ , \tag{A.7}$$

and the parallel current density, $J_{||}$, is determined from the scalar product of Eq.(A.2) with $\widehat{\mathbf{b}} \equiv \mathbf{B}/B$

$$J_{||} = \frac{\sigma_{||}}{en} \left(\nabla_{||} p_e + c_1 n \nabla_{||} T_e - en \nabla_{||} \Phi \right) \ . \tag{A.8}$$

Combining Eqs.(A.6-A.8) and linearizing, we obtain the quasineutrality equation (for $V_{i||} \ll V_{e||}$) as

$$\frac{n_0 c}{B \omega_{ci}} \, \frac{\partial}{\partial t} \, \nabla_{\perp}^2 \Phi = 2 n_0 \frac{\boldsymbol{\nabla} B}{B} \cdot \mathbf{V}_{\star e} + \mathbf{B} \cdot \boldsymbol{\nabla} \left[\frac{\sigma_{||}}{en_0 B} \left(\nabla_{||} p_e + c_1 n \nabla_{||} T_e - en \nabla_{||} \Phi \right) \right] \ , \tag{A.9}$$

where we made use of the (low-β) relation of

$$\boldsymbol{\nabla}\cdot\frac{\mathbf{B}\times\boldsymbol{\nabla}f}{B^2} \simeq -2\frac{\boldsymbol{\nabla}B}{B}\cdot\frac{\mathbf{B}\times\boldsymbol{\nabla}f}{B^2} \ , \tag{A.10}$$

for any fluctuating quantity f. Using the definitions (A.5) in the electron continuity equation

$$\frac{\partial n}{\partial t} = -\boldsymbol{\nabla}\cdot\left(n\mathbf{V}_E\right) - \boldsymbol{\nabla}\cdot\left(n\mathbf{V}_{\star e}\right) - \boldsymbol{\nabla}\cdot\left(n\mathbf{V}_c\right) \ , \tag{A.11}$$

and noting that $V_c \sim V_E/\left(\omega_{ce}\tau_e\right) \ll V_E \sim V_{\star e}$, one gets

$$\frac{\partial n}{\partial t} = \left(2\frac{\boldsymbol{\nabla}B}{B} + \frac{\boldsymbol{\nabla}\rho}{L_n}\right)\cdot\left(n_0\mathbf{V}_E\right) + 2\frac{\boldsymbol{\nabla}B}{B}\cdot\left(n_0\mathbf{V}_E\right) + \frac{1}{e}\,\mathbf{B}\cdot\boldsymbol{\nabla}\left(\frac{J_{||}}{B}\right) \ . \tag{A.12}$$

Here $\rho = \rho(\psi)$ is a radial coordinate ($\mathbf{B}\cdot\boldsymbol{\nabla}\rho = 0$). In drift wave units [$\overline{t} = \omega_\star t, \omega_\star = c_s/L_n$ is the drift frequency, $c_s = \sqrt{T_e/m_i}$ is the sound speed, $(\widetilde{n}\ , \widetilde{\Phi}) = (\delta n/n_0, e\Phi/T_e)$], Eqs.(A.9,A.12) become

$$\frac{1}{\overline{B}^2}\,\frac{\partial\overline{\omega}}{\partial\overline{t}} = 2\xi\overline{B}L_n\nabla_{||}\left(\frac{L_n}{\overline{B}}\,\nabla_{||}\widetilde{g}\right) - 2\mathbf{Q}\cdot\frac{\widehat{\mathbf{b}}\times\rho_{\mathrm{s0}}\boldsymbol{\nabla}\left(\widetilde{n} + \widetilde{T}_e\right)}{\overline{B}} \tag{A.13}$$

and

$$\frac{\partial\widetilde{n}}{\partial\overline{t}} = \boldsymbol{\nabla}\rho\cdot\frac{\widehat{\mathbf{b}}\times\rho_{\mathrm{s0}}\boldsymbol{\nabla}\widetilde{\Phi}}{\overline{B}} - 2\mathbf{Q}\cdot\frac{\widehat{\mathbf{b}}\times\rho_{\mathrm{s0}}\boldsymbol{\nabla}\left(\widetilde{h} + \widetilde{T}_e\right)}{\overline{B}} + 2\xi\overline{B}L_n\nabla_{||}\left(\frac{L_n}{\overline{B}}\,\nabla_{||}\widetilde{g}\right) \tag{A.14}$$

where $\overline{\omega} \equiv {\rho_{\mathrm{s0}}}^2\nabla_\perp^2\widetilde{\Phi}$ and $\xi \equiv \omega_\star\tau_e\left(m_i/m_e\right) \gg 1$ is termed the collisional parameter; $\mathbf{Q} \equiv L_n\boldsymbol{\nabla}B/B$ is related to the curvature of the magnetic field and $\rho_{\mathrm{s0}} = \sqrt{T_e/m_i}/\left(eB_0/m_ic\right)$; $\overline{B} \equiv B/B_0$ where B_0 is a magnetic field of reference (see main text); $\widetilde{g} = \widetilde{h} + (1+c_1)\widetilde{T}_e$; finally $\widetilde{h} = \widetilde{n} - \widetilde{\Phi}$ is the nonadiabatic response of the electrons. The electron energy equation [7] is given by

$$\frac{3}{2}\,n\left(\frac{\partial}{\partial t} + \mathbf{V}_e\cdot\boldsymbol{\nabla}\right)T_e = -p_e\boldsymbol{\nabla}\cdot\mathbf{V}_e - \boldsymbol{\nabla}\cdot\mathbf{q}_e + Q_{ei} \ , \tag{A.15}$$

where Q_{ei} is the electron heating and

$$\mathbf{q}_e = -c_1p_e\frac{J_{||}}{en} - \frac{3}{2}\,\frac{p_e}{\omega_{ce}\tau_{\mathrm{e}}}\,\widehat{\mathbf{b}}\times\left(\frac{\mathbf{J}_\perp}{en}\right) - \chi_{||}\boldsymbol{\nabla}_{||}T_e - \chi_\perp\boldsymbol{\nabla}_\perp T_e - \chi_\star\widehat{\mathbf{b}}\times\boldsymbol{\nabla}T_e \ , \tag{A.16}$$

is the electron heat flux; here $\chi_{||} = c_2\chi_0$, $\chi_\perp = c_3\chi_0/\left(\omega_{ce}\tau_{\mathrm{e}}\right)^2$, $\chi_\star = \frac{5}{2}\,\chi_0/\left(\omega_{ce}\tau_{\mathrm{e}}\right)$, $\chi_0 = n_0T_e\tau_e/m_e$ and $\omega_{ce}\tau_{\mathrm{e}} \gg 1$ for typical plasma edge parameters; the coefficients are $c_2 = 3.2$ and $c_3 = 4.7$. Neglecting higher-order terms the divergence of the electron heat flux is

$$\begin{aligned}\boldsymbol{\nabla}\cdot\mathbf{q}_e &= -c_1\frac{T_e}{e}\,\mathbf{B}\cdot\boldsymbol{\nabla}\left(\frac{J_{||}}{B}\right) - \chi_{||}\mathbf{B}\cdot\boldsymbol{\nabla}\left(\frac{1}{B}\,\nabla_{||}T_e\right) \\ &+ \chi_\star\left(2\frac{\boldsymbol{\nabla}B}{B} - \frac{\boldsymbol{\nabla}p_e}{p_e}\right)\cdot\left(\widehat{\mathbf{b}}\times\boldsymbol{\nabla}T_e\right) \ .\end{aligned} \tag{A.17}$$

whereas the divergence of the electron fluid velocity is

$$\boldsymbol{\nabla}\cdot\mathbf{V}_e = \boldsymbol{\nabla}\cdot\mathbf{V}_{e||} - \mathbf{V}_{\star e}\cdot\frac{\boldsymbol{\nabla}n}{n} + \frac{1}{n}\,\boldsymbol{\nabla}\cdot\left(n\mathbf{V}_{\star e}\right) + \boldsymbol{\nabla}\cdot\mathbf{V}_E \ , \tag{A.18}$$

where the small term $\boldsymbol{\nabla}\cdot\mathbf{V}_c$ has been neglected. Using Eqs.(A.17,A.18) one can write Eq.(A.15) as

$$\frac{3}{2}\,n\frac{\partial T_e}{\partial t}\;+\frac{3}{2}\,n\mathbf{V}_E\cdot\boldsymbol{\nabla}T_e+\frac{3}{2}\,n\mathbf{V}_{\star e}\cdot\boldsymbol{\nabla}T_e=T_e\mathbf{V}_{\star e}\cdot\boldsymbol{\nabla}n-p_e\boldsymbol{\nabla}\cdot\mathbf{V}_{e||}-p_e\boldsymbol{\nabla}\cdot\mathbf{V}_E \tag{A.19}$$

$$-T_e\cdot\boldsymbol{\nabla}\left(n\mathbf{V}_{\star e}\right)+c_1\frac{T_e}{e}\,\mathbf{B}\cdot\boldsymbol{\nabla}\left(\frac{J_{||}}{B}\right)+\chi_{||}\mathbf{B}\cdot\boldsymbol{\nabla}\left(\frac{1}{B}\,\nabla_{||}T_e\right)$$

$$-\chi_\star\left(2\frac{\boldsymbol{\nabla}B}{B}\right)\cdot\left(\widehat{\mathbf{b}}\times\boldsymbol{\nabla}T_e\right)+\chi_\star\frac{\boldsymbol{\nabla}p_e}{p_e}\cdot\left(\widehat{\mathbf{b}}\times\boldsymbol{\nabla}T_e\right)\;. \tag{A.20}$$

The last term on the left-hand side of Eq.(A.19) cancels with the sum of the first and last terms on the right-hand side of that equation since

$$\chi_\star\frac{\boldsymbol{\nabla}p_e}{p_e}\cdot\left(\widehat{\mathbf{b}}\times\boldsymbol{\nabla}T_e\right)=\frac{5}{2}\,n\mathbf{V}_{\star e}\cdot\boldsymbol{\nabla}T_e\;, \tag{A.21}$$

and $n\mathbf{V}_{\star e}\cdot\boldsymbol{\nabla}T_e+T_e\mathbf{V}_{\star e}\cdot\boldsymbol{\nabla}n=\mathbf{V}_{\star e}\cdot\boldsymbol{\nabla}p_e\equiv 0$. With these simplicifications Eq.(A.19) takes the form of

$$\begin{aligned}\underbrace{\frac{3}{2}\,n\frac{\partial T_e}{\partial t}}_{\mathbf{1}} &= \underbrace{-\frac{3}{2}\,n\mathbf{V}_E\cdot\boldsymbol{\nabla}T_e}_{\mathbf{2}}-\underbrace{p_e\boldsymbol{\nabla}\cdot\mathbf{V}_{e||}}_{\mathbf{3}}-\underbrace{p_e\boldsymbol{\nabla}\cdot\mathbf{V}_E}_{\mathbf{4}}-\underbrace{T_e\boldsymbol{\nabla}\cdot\left(n\mathbf{V}_{\star e}\right)}_{\mathbf{5}}\\ &+\underbrace{c_1\frac{T_e}{e}\,\mathbf{B}\cdot\boldsymbol{\nabla}\left(\frac{J_{||}}{B}\right)}_{\mathbf{6}}+\underbrace{\chi_{||}\mathbf{B}\cdot\boldsymbol{\nabla}\left(\frac{1}{B}\,\nabla_{||}T_e\right)}_{\mathbf{7}}\\ &-\underbrace{2\chi_\star\frac{\boldsymbol{\nabla}B}{B}\cdot\left(\widehat{\mathbf{b}}\times\boldsymbol{\nabla}T_e\right)}_{\mathbf{8}}\end{aligned} \tag{A.22}$$

Term **2** represents the tapping of free energy contained in the temperature gradient by the drift wave. Terms **4**, **5** and **8** are curvature terms; the remaining terms are related to the transport of heat along the field lines. The plasma density and the electron temperature are written as $n=n_0+\delta n$ and $T_e=T_{e0}+\delta T_e$ where a subscript '0' denotes the equilibrium part and δn and δT_e are perturbations. Using Eq.(A.10), one can write Eq.(A.22) as

$$\begin{aligned}\frac{3}{2}\,\frac{\partial\widetilde{T}_e}{\partial\widetilde{t}} &= \frac{3}{2}\,\eta_e\boldsymbol{\nabla}\rho\cdot\frac{\widehat{\mathbf{b}}\times\rho_{\mathrm{s0}}\boldsymbol{\nabla}\widetilde{\Phi}}{\overline{B}}\;+\overline{B}L_n\nabla_{||}\left(\frac{\widetilde{J_{||}}}{\overline{B}}\right)+2\mathbf{Q}\cdot\frac{\widehat{\mathbf{b}}\times\rho_{\mathrm{s0}}\boldsymbol{\nabla}\widetilde{\Phi}}{\overline{B}}\\ &-2\mathbf{Q}\cdot\frac{\widehat{\mathbf{b}}\times\rho_{\mathrm{s0}}\boldsymbol{\nabla}\left(\widetilde{n}\;+\widetilde{T}_e\right)}{\overline{B}}\;+c_1\overline{B}L_n\nabla_{||}\left(\frac{\widetilde{J_{||}}}{\overline{B}}\right)\\ &+c_2\xi\overline{B}L_n\nabla_{||}\left(\frac{L_n\nabla_{||}\widetilde{T}_e}{\overline{B}}\right)-\frac{5}{2}\,\frac{2\mathbf{Q}}{\overline{B}}\cdot\left(\widehat{\mathbf{b}}\times\rho_{\mathrm{s0}}\boldsymbol{\nabla}\widetilde{T}_e\right)\;,\end{aligned} \tag{A.23}$$

where $\mathbf{Q}\equiv L_n\boldsymbol{\nabla}B/B\sim L_n/L_B\sim L_n/R_0=\epsilon_n$. Noting that the parallel current density is given by $\widetilde{J_{||}}=2\xi L_n\nabla_{||}\widetilde{g}$ and rearranging the terms in the above equation, one obtains

$$\frac{\partial\widetilde{T}_e}{\partial\widetilde{t}}\;=\eta_e\boldsymbol{\nabla}\rho\cdot\frac{\widehat{\mathbf{b}}\times\rho_{\mathrm{s0}}\boldsymbol{\nabla}\widetilde{\Phi}}{\overline{B}}\;+2\xi\overline{B}L_n\nabla_{||}\left(\frac{L_n\nabla_{||}\widetilde{\varphi}}{\overline{B}}\right)-\frac{4}{3}\,\mathbf{Q}\cdot\frac{\widehat{\mathbf{b}}\times\rho_{\mathrm{s0}}\boldsymbol{\nabla}\widetilde{\psi}}{\overline{B}}\;, \tag{A.24}$$

where $\widetilde{\varphi}\equiv\frac{2}{3}\,(1+c_1)\widetilde{g}\;+\frac{c_2}{3}\,\widetilde{T}_e$, $\widetilde{g}\;\equiv\widetilde{h}\;+(1+c_1)\widetilde{T}_e$ and $\widetilde{\psi}=\widetilde{h}\;+\frac{7}{2}\,\widetilde{T}_e$.

Appendix: Remarks on the Local Magnetic Shear

Using the definitions of the unit parallel vector, $\widehat{\mathbf{b}} = \mathbf{B}/B$, and the unit normal vector, $\widehat{\mathbf{n}} = \boldsymbol{\nabla}\psi/\sqrt{g^{\psi\psi}}$, we can write the binormal vector as

$$\widehat{\mathbf{g}} = f\left(\mathbf{B}\times\boldsymbol{\nabla}\psi\right) \ , \tag{B.25}$$

where $f = \left(B\sqrt{g^{\psi\psi}}\right)^{-1}$. Using Eq.(B.25) in the definition of the local magnetic shear we obtain

$$\begin{aligned} S &= \widehat{\mathbf{g}}\cdot\boldsymbol{\nabla}\times\widehat{\mathbf{g}} = \widehat{\mathbf{g}}\cdot\left[\boldsymbol{\nabla}f\times\left(\mathbf{B}\times\boldsymbol{\nabla}\psi\right) + \boldsymbol{\nabla}\times\left(\mathbf{B}\times\boldsymbol{\nabla}\psi\right)\right] \ , \\ &= f(\boldsymbol{\nabla}g^{\psi\psi}\cdot\underbrace{\boldsymbol{\nabla}\alpha\times\widehat{\mathbf{g}}}_{\mathbf{1}} - \boldsymbol{\nabla}g^{\alpha\psi}\underbrace{\boldsymbol{\nabla}\psi\times\widehat{\mathbf{g}}}_{\mathbf{2}}) \ , \end{aligned} \tag{B.26}$$

where we have used the Clebsch for the magnetic field, $\mathbf{B} = \boldsymbol{\nabla}\alpha\times\boldsymbol{\nabla}\psi$. Terms **1** and **2** in Eq.(B.26) can be written as

$$\boldsymbol{\nabla}\alpha\times\widehat{\mathbf{g}} = g\boldsymbol{\nabla}\alpha\times\left(\mathbf{B}\times\boldsymbol{\nabla}\psi\right) = fg^{\alpha\psi}\mathbf{B} \ , \tag{B.27}$$

and

$$\boldsymbol{\nabla}\psi\times\widehat{\mathbf{g}} = f\boldsymbol{\nabla}\psi\times\left(\mathbf{B}\times\boldsymbol{\nabla}\psi\right) = \frac{\sqrt{g^{\psi\psi}}}{B}\,\mathbf{B} \ , \tag{B.28}$$

respectively. Combining Eqs.(B.26-B.28), one can write

$$\begin{aligned} S &= f\left(fg^{\alpha\psi}\mathbf{B}\cdot\boldsymbol{\nabla}g^{\psi\psi} - \frac{\sqrt{g^{\psi\psi}}}{B}\,\mathbf{B}\cdot\boldsymbol{\nabla}g^{\alpha\psi}\right) \ , \\ &= -\frac{\left|\boldsymbol{\nabla}\psi\right|^2}{B^2}\,\mathbf{B}\cdot\boldsymbol{\nabla}\left(\frac{g^{\alpha\psi}}{g^{\psi\psi}}\right) \ , \\ &= \frac{\left|\boldsymbol{\nabla}\psi\right|^2}{B^2}\,\mathbf{B}\cdot\boldsymbol{\nabla}\left(D + \zeta\frac{d\iota}{d\psi}\right) \ , \end{aligned} \tag{B.29}$$

where

$$D \equiv \frac{\iota\boldsymbol{\nabla}\zeta\cdot\boldsymbol{\nabla}\psi - \boldsymbol{\nabla}\theta\cdot\boldsymbol{\nabla}\psi}{\boldsymbol{\nabla}\psi} \ . \tag{B.30}$$

Appendix: Jacobian for the Helical Parameterization

In this Appendix, we consider the case of a configuration with a helical axis

$$\begin{aligned} R &= R_0 + \rho\cos\theta + \Delta\cos\left(N_p\zeta\right) \ , \\ \phi &= -\zeta \ , \\ Z &= \rho\sin\theta + \Delta\sin\left(N_p\zeta\right) \ , \end{aligned} \tag{C.31}$$

where Δ is a measure of the helical excursion of the magnetic axis. Using the helical parameterization (C.31), we obtain the following covariant metric elements

$$\begin{aligned} g_{\theta\theta} &= \rho^2 \ , \\ g_{\theta\zeta} &= N_p\rho\Delta\cos\left(N_p\zeta-\theta\right) \ , \\ g_{\zeta\zeta} &= R^2 + N_p^2\Delta^2 \ . \end{aligned} \tag{C.32}$$

The Jacobian constraint equation is given by

$$\frac{\partial}{\partial\theta}\left(\frac{F}{\mathcal{J}}\right) = \frac{\partial}{\partial\zeta}\left(\frac{G}{\mathcal{J}}\right) \ , \tag{C.33}$$

where $F(\theta,\zeta) = g_{\zeta\zeta} + \iota g_{\theta\zeta} = R^2 + N_p^2\Delta^2 + N_p\rho\Delta\iota\cos\varphi$ and $G(\theta,\zeta) = g_{\theta\zeta} + \iota g_{\theta\theta} = \iota\rho^2 + N_p\rho\Delta\cos\varphi$, where $\varphi \equiv N_p\zeta - \theta$ is the helical coordinate. Using the change of variable $(\theta,\zeta) \mapsto \left(\varphi,\overline{\theta}\right)$ with

$$\begin{aligned} \varphi &= N_p\zeta - \theta \ , \\ \overline{\theta} &= \theta \ , \end{aligned} \tag{C.34}$$

in Eq.(C.33), we arrive at

$$\frac{\partial}{\partial\theta}\left(\frac{F}{\mathcal{J}}\right) = \frac{\partial}{\partial\varphi}\left(\frac{N_pG+F}{\mathcal{J}}\right) \ , \tag{C.35}$$

where $\overline{\theta} \equiv \theta$. Let $X(\theta) = R_0 + \rho\cos\theta$. For $\Delta = 0$, we have the relations of $F = X^2(\theta)$ and $G = \iota\rho^2$. The Jacobian constraint admits the exact solution of $\mathcal{J} = CX^2(\theta)$, where C is a constant. Let us seek a solution of the form

$$\mathcal{J} = \frac{X^2(\theta)}{A(\varphi)} \ . \tag{C.36}$$

Substituting the trial function (C.36) in Eq.(C.35) we obtain

$$\left(N_pG+F\right)\frac{dA}{d\varphi} = f\left(\theta,\zeta\right)A\left(\varphi\right) \ , \tag{C.37}$$

where

$$f\left(\theta,\zeta\right) = 2\rho\sin\theta\left(\frac{F}{X} - R\right) + N_p\left(N_p+\iota\right)\rho\Delta\sin\varphi \ . \tag{C.38}$$

We can write $R = R_0\left[1 + \epsilon_{\rm t}\cos\theta + \epsilon_{\rm h}\cos\left(N_p\zeta\right)\right]$ where $\epsilon_{\rm t} \equiv \rho/R_0$ and $\epsilon_{\rm h} \equiv \Delta/R_0$ are termed the toroidal parameter anf the helical parameter, respectively. After some algebra, we obtain the relation of

$$\begin{aligned} \frac{F}{X} - R &\simeq R_0\left\{\epsilon_{\rm h}\cos\left(\varphi+\theta\right) + \left(N_p^2{\epsilon_{\rm h}}^2 + N_p\epsilon_{\rm t}\epsilon_{\rm h}\iota\cos\varphi\right)\left(1-\epsilon_{\rm t}\cos\theta\right)\right. \\ &+ \left.{\epsilon_{\rm h}}^2\cos^2\left(\varphi+\theta\right)\left(1-\epsilon_{\rm t}\cos\theta\right)\right\} \ . \end{aligned} \tag{C.39}$$

Introducing the operator

$$\overline{F} \equiv \frac{1}{2\pi} \int_0^{2\pi} F(\theta) d\theta \ , \tag{C.40}$$

and noting the relations of

$$\begin{aligned} \overline{\cos(\varphi+\theta)\sin\theta} &= -\frac{\sin\varphi}{2} \ , \\ \overline{\cos^2(\varphi+\theta)\sin\theta} &= 0 \ , \\ \overline{\cos\theta\sin\theta\cos^2(\varphi+\theta)} &= -\frac{1}{4}\cos\varphi\sin\varphi \ , \end{aligned}$$

one can show that

$$\overline{f} = -R_0\rho\epsilon_{\rm h}\sin\varphi\left(1-\frac{\widehat{\epsilon}}{2}\cos\varphi\right) + N_p\left(N_p+\iota\right)\rho\Delta\sin\varphi \ , \tag{C.41}$$

where $\widehat{\epsilon} \equiv \epsilon_{\rm t}\epsilon_{\rm h}$. Similarly one has

$$\overline{R^2} = R_0^2\left(1+\frac{{\epsilon_{\rm t}}^2}{2}+\widehat{\epsilon}\cos\varphi+\frac{{\epsilon_{\rm h}}^2}{2}\right) \ , \tag{C.42}$$

$$\overline{F} = R_0^2\left[1+\frac{{\epsilon_{\rm t}}^2}{2}+\left(N_p^2+\frac{1}{2}\right){\epsilon_{\rm h}}^2+\widehat{\epsilon}(1+N_p\iota)\cos\varphi\right] \ , \tag{C.43}$$

and

$$\overline{G} = R_0^2\left(N_p\widehat{\epsilon}\cos\varphi+\iota{\epsilon_{\rm t}}^2\right) \ . \tag{C.44}$$

Using Eqs.(C.41-C.44), we obtain the relation of

$$\left(\widehat{\alpha}+\widehat{\beta}\cos\varphi\right)\frac{dA}{d\varphi} = \xi\sin\varphi A \ , \tag{C.45}$$

where $\widehat{\alpha} = 1+{\epsilon_{\rm t}}^2\left(N_p\iota+\frac{1}{2}\right)+{\epsilon_{\rm h}}^2\left(N_p^2+\frac{1}{2}\right)$, $\widehat{\beta} = \widehat{\epsilon}\left[1+N_p\left(N_p+\iota\right)\right]$ and $\xi = \left[N_p\left(N_p+\iota\right)-1\right]\widehat{\epsilon}$. Eq.(C.45) can be solved perturbatively in ascending order of the smallness parameter $\epsilon \equiv N_p^2\widehat{\epsilon}$ by writing

$$A = A_0 + A_1\epsilon + A_2\epsilon^2 + \cdots \tag{C.46}$$

We have the relations of

$$\widehat{\alpha}\frac{dA_0}{d\varphi} = 0 \qquad \left[\mathcal{O}\left(\epsilon^0\right)\right] \ , \tag{C.47}$$

$$\widehat{\beta}\cos\varphi\frac{dA_0}{d\varphi} + \widehat{\alpha}\frac{dA_1}{d\varphi} = A_0\xi\sin\varphi \qquad \left[\mathcal{O}\left(\epsilon\right)\right] \ , \tag{C.48}$$

and

$$\widehat{\beta}\frac{dA_2}{d\varphi} + \widehat{\beta}\cos\varphi\frac{dA_1}{d\varphi} = A_1\xi\sin\varphi \qquad \left[\mathcal{O}\left(\epsilon^2\right)\right] \ . \tag{C.49}$$

Eqs.(C.47-C.49) can be solved with the result of

$$A_0 = \text{const} \ ,$$

$$A_1 = A_0 \frac{\xi}{\widehat{\alpha}} \ (1 - \cos\varphi) \ ,$$

and

$$A_2 = A_0 \frac{\xi}{\widehat{\alpha}^2} \ \left[\xi \, (1 - \cos\varphi) - \frac{\widehat{\beta} + \xi}{2} \ \sin^2 \varphi \right] \ .$$

It follows that the Jacobian can be written as

$$\mathcal{J} = \frac{X^2 \, (\theta)}{A_0 \, (\psi) \, g \, (\varphi)} \ , \tag{C.50}$$

where $g \, (\varphi) = 1 + a \, (1 - \cos\varphi) - b \sin^2 \varphi$, $a = \xi(1 + \xi/\widehat{\alpha})/\widehat{\alpha}$ and $b = \xi(\widehat{\beta} + \xi)/(2\widehat{\alpha}^2)$.

Acknowledgments This research was supported by Contract No. DE-AC02-CH0-3073 and the Scientific Discovery through Advanced Computing (SciDAC) initiative (U.S. Department of Energy).

References

1. W. Horton, Rev. Mod. Phys. **71**, 735 (1999).
2. J.W. Connor, R.J. Hastie and J.B. Taylor, Proc. Roy. Soc. London **A 365**, 1 (1979).
3. C.C. Hegna, Phys. Plasmas **7**(10), 3921 (2000).
4. R. Courant, K. Friedrichs and H. Lewy, Mathematische Annalen **100**, 32 (1928).
5. J.L.V. Lewandowski, *Drift wave models for three-dimensional plasmas* (Ph.D. Thesis, the Australian National University, 1997).
6. M. Persson, J. L. V. Lewandowski and H. Nordman, Phys. Plasmas **2**(9), 3440 (1996).
7. S.I. Braginskii,in *Review of Plasma Physics*, edited by M.A. Leontovitch (Consultants Bureau, N.Y., 1965).
8. A. Zagorodny and J. Weiland, Phys. Plasmas **6**(6), 2359 (1999).
9. D.W. Peaceman and H.H. Rachford, J. Soc. Indust. Applied Mathematics **3**(1), 28 (1955).
10. J.L.V. Lewandowski, Phys. Plasmas **7**(8), 3360 (2000).
11. M. Nadeem, T. Rafiq and M. Persson, Phys. Plasmas **8**(10), 4375 (2001).

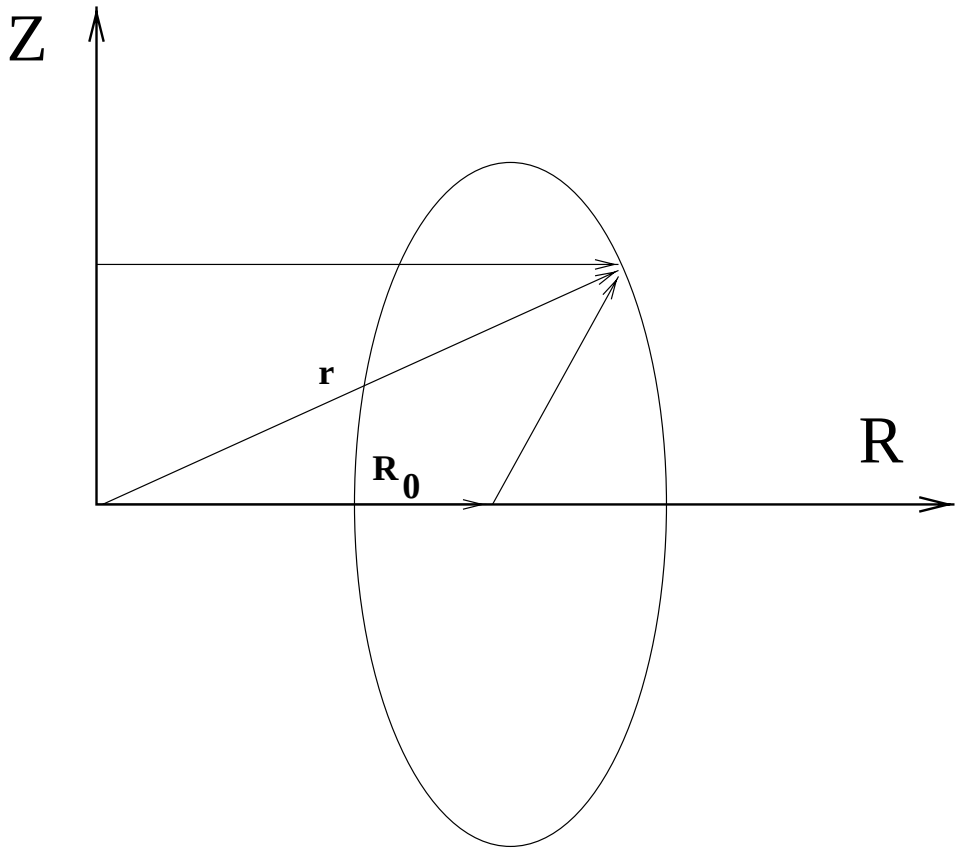

Fig. 1. Schematic representation of the cross section $\zeta = 0$ (see main text for definition of the average minor radius, $\overline{a}$).

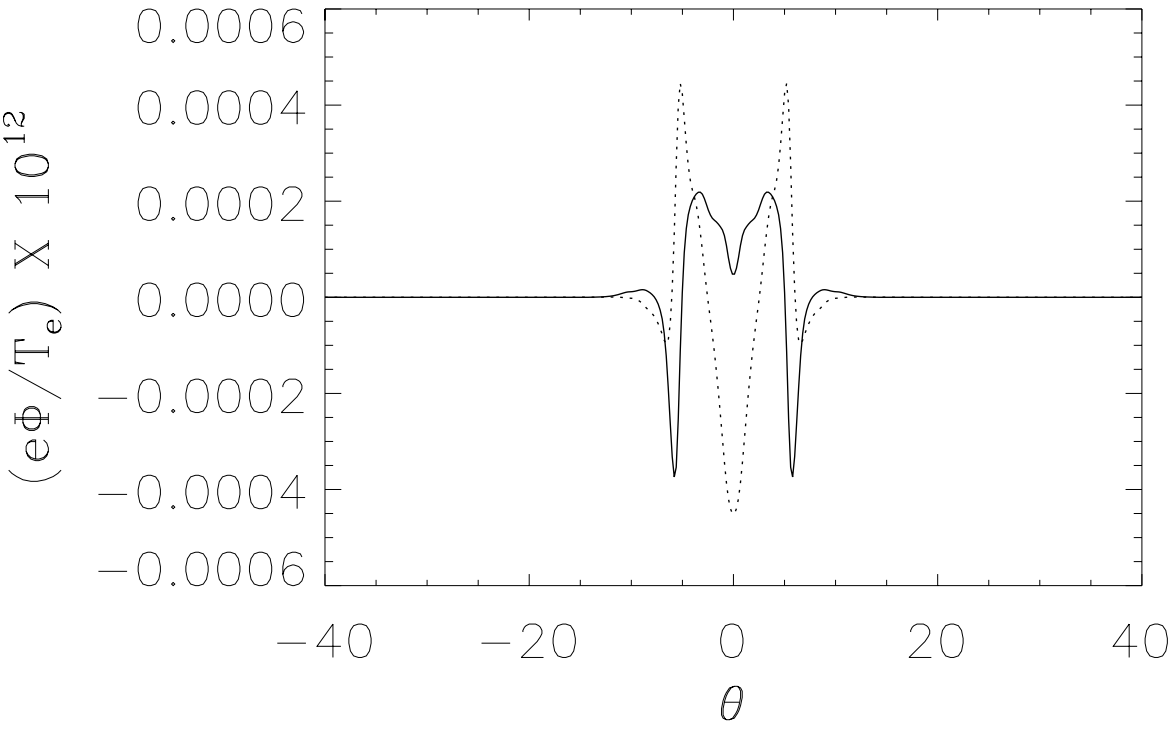

Fig. 2. Real (plain line) and imaginary (dotted line) parts of the mode amplitude for the normalized electrostatic potential at saturation, $\omega_\star t = 250$.

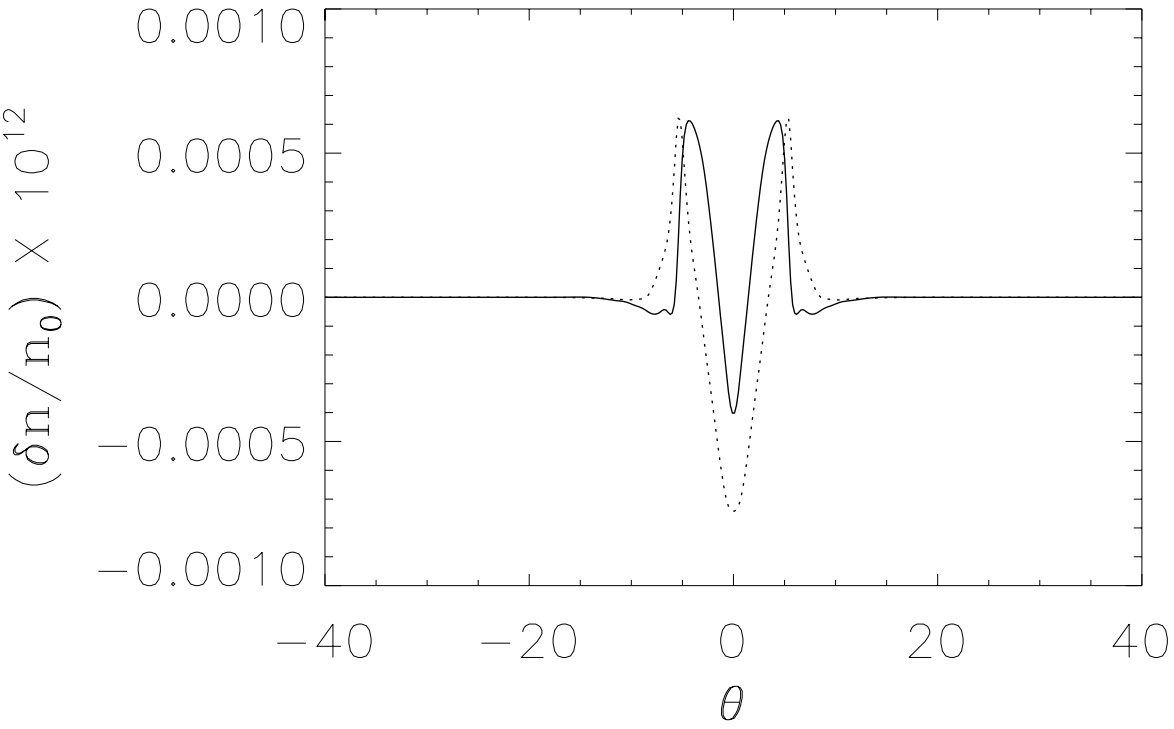

Fig. 3. Real (plain line) and imaginary (dotted line) parts of the mode amplitude for the normalized perturbed plasma density at saturation, $\omega_\star t = 250$.

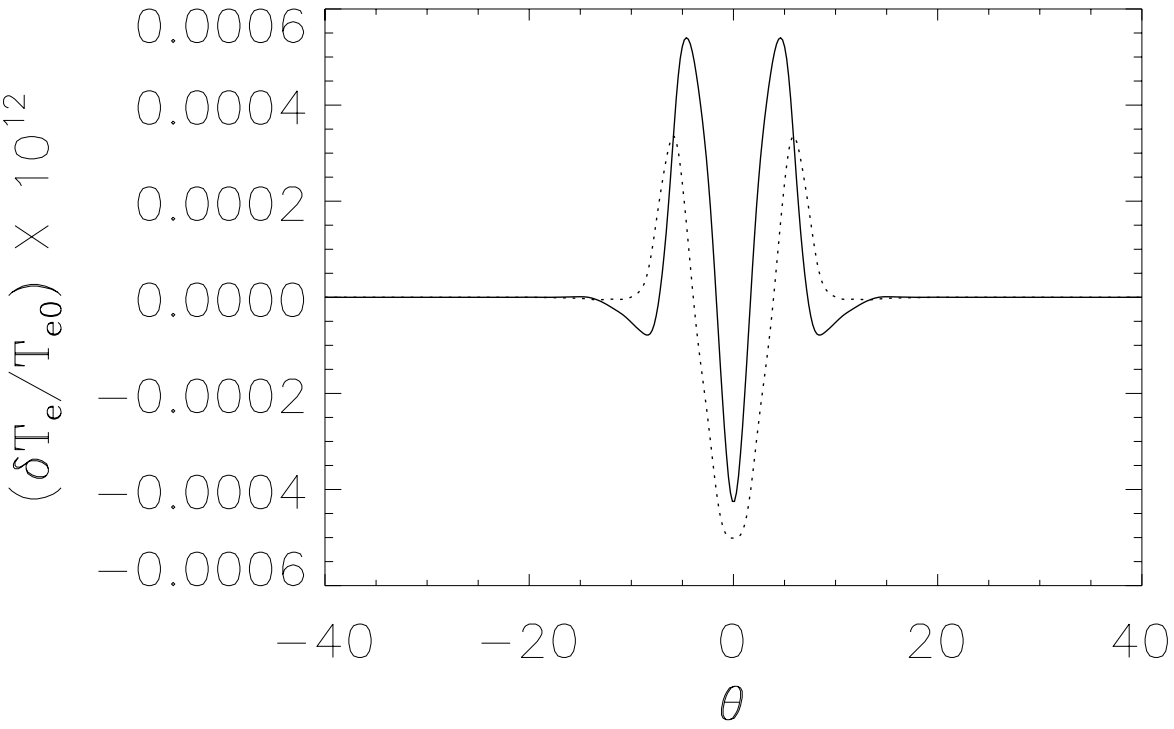

Fig. 4. Real (plain line) and imaginary (dotted line) parts of the mode amplitude for the normalized perturbed electron temperature at saturation, $\omega_\star t = 250$.

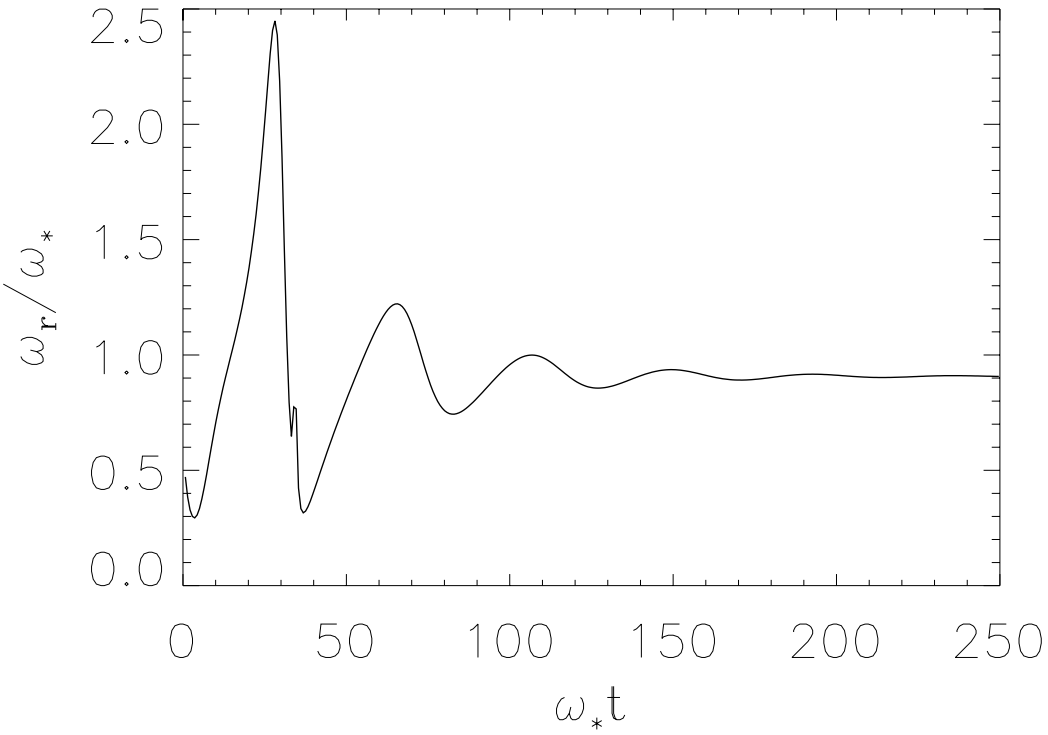

Fig. 5. Average real mode frequency as a function of the normalized time $\overline{t} = \omega_\star t$.

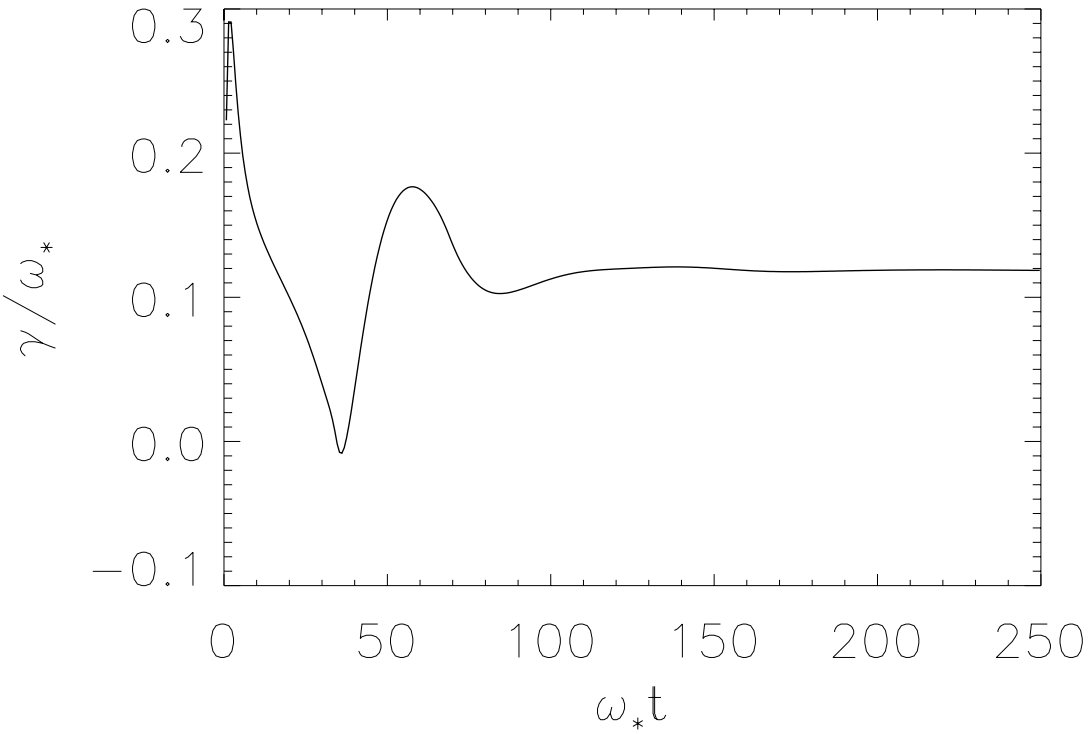

Fig. 6. Average linear growth rate as a function of the normalized time $\overline{t} = \omega_\star t$.

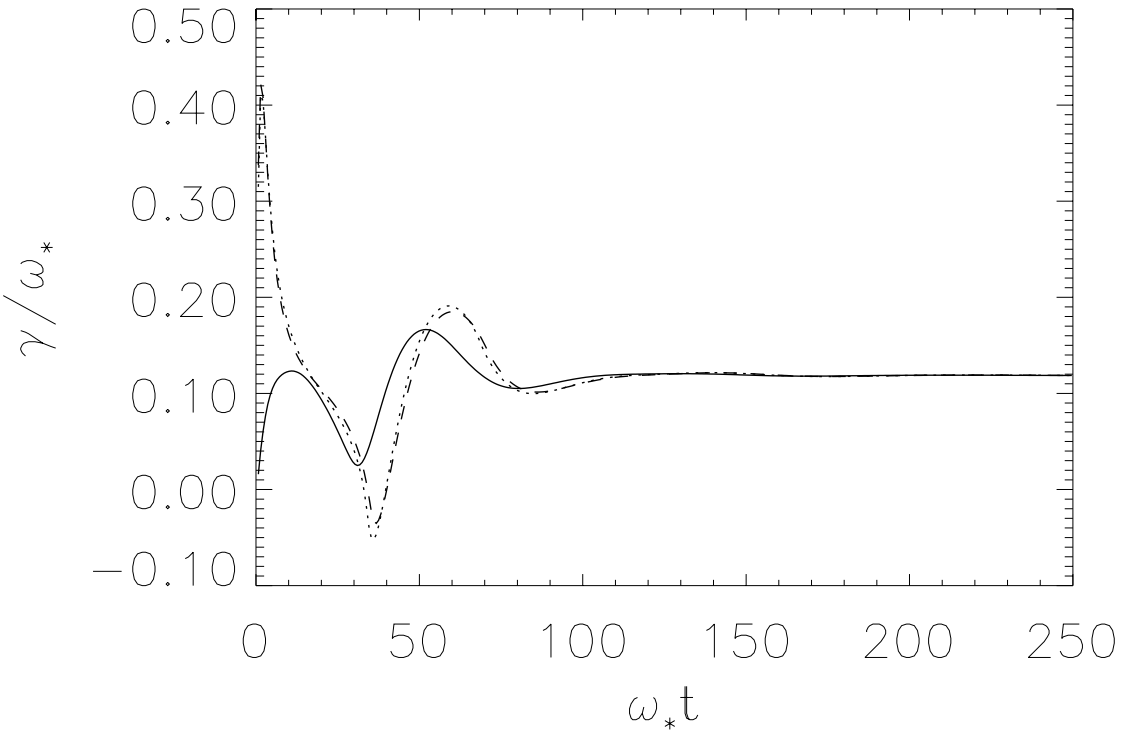

Fig. 7. Instantaneous linear growth rates for the electrostatic potential (plain line), the perturbed plasma density (dotted line) and the perturbed electron temperature (dashed line) as a function of the normalized time $\overline{t} = \omega_\star t$.

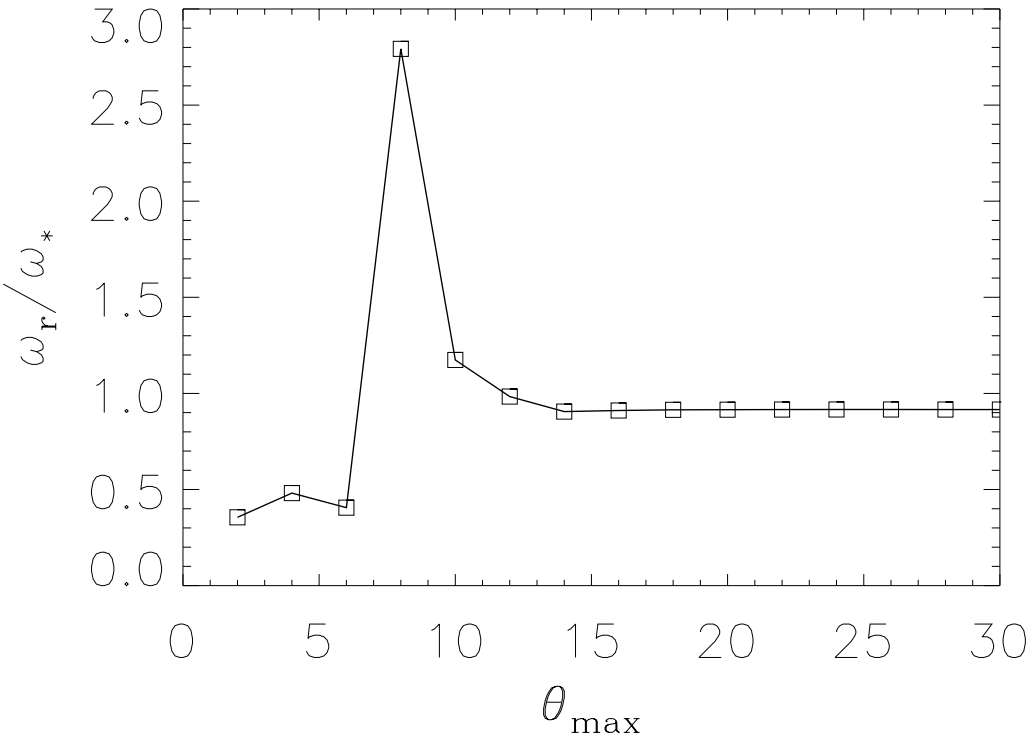

Fig. 8. Average real mode frequency as a function of the parameter $\theta_{\max}$.

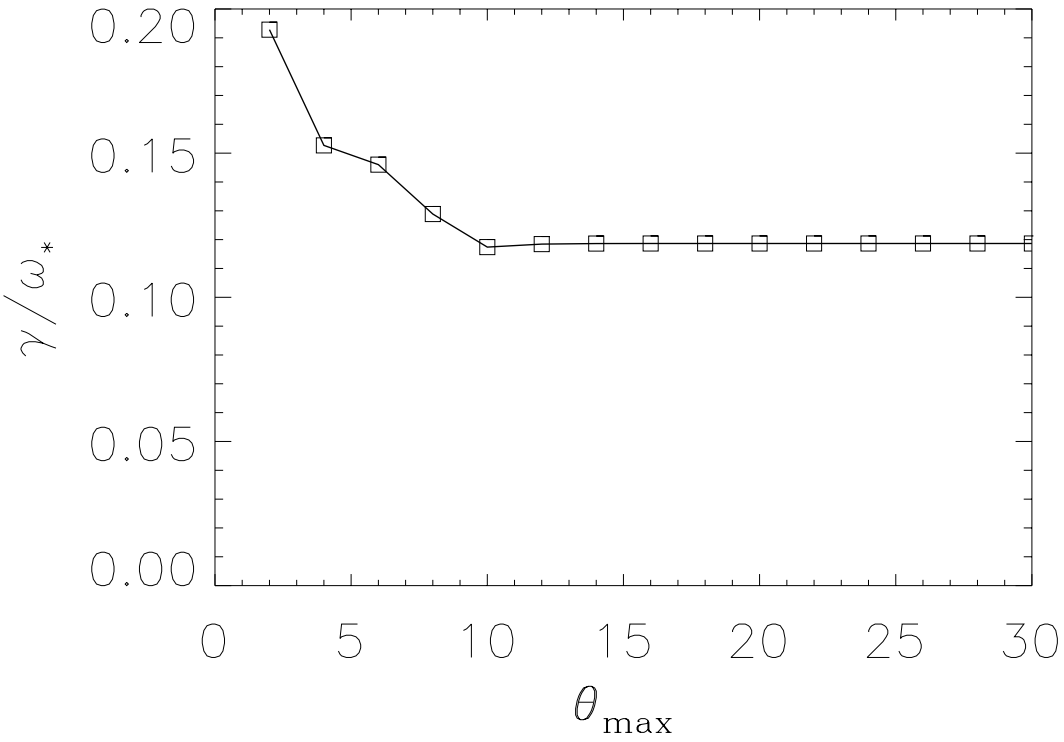

Fig. 9. Average linear growth rate as a function of the parameter $\theta_{\max}$.

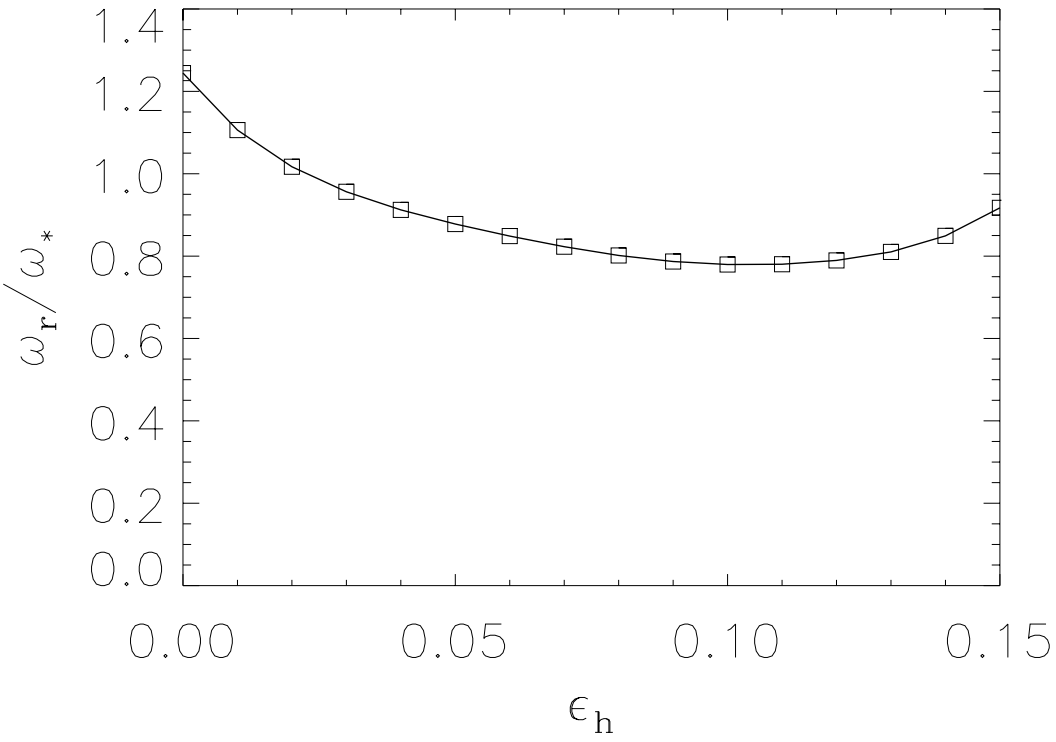

Fig. 10. Average real mode frequency at saturation as a function of the helical parameter ϵ_h.

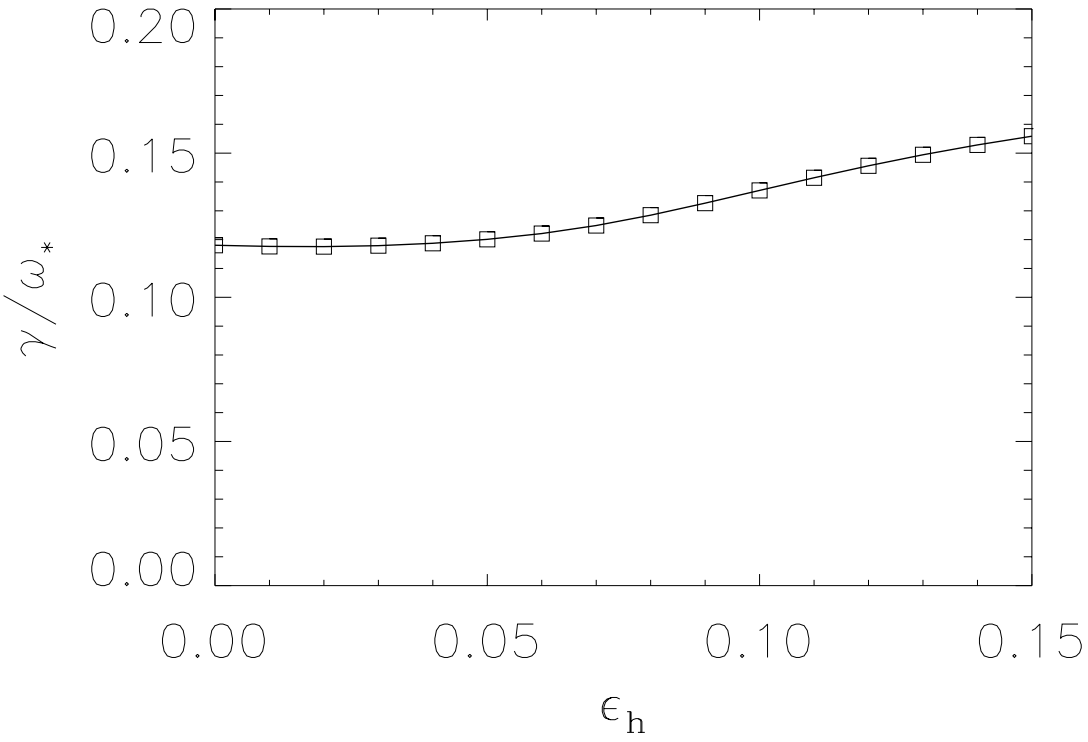

Fig. 11. Average linear growth rate at saturation as a function of the helical parameter ϵ_h.

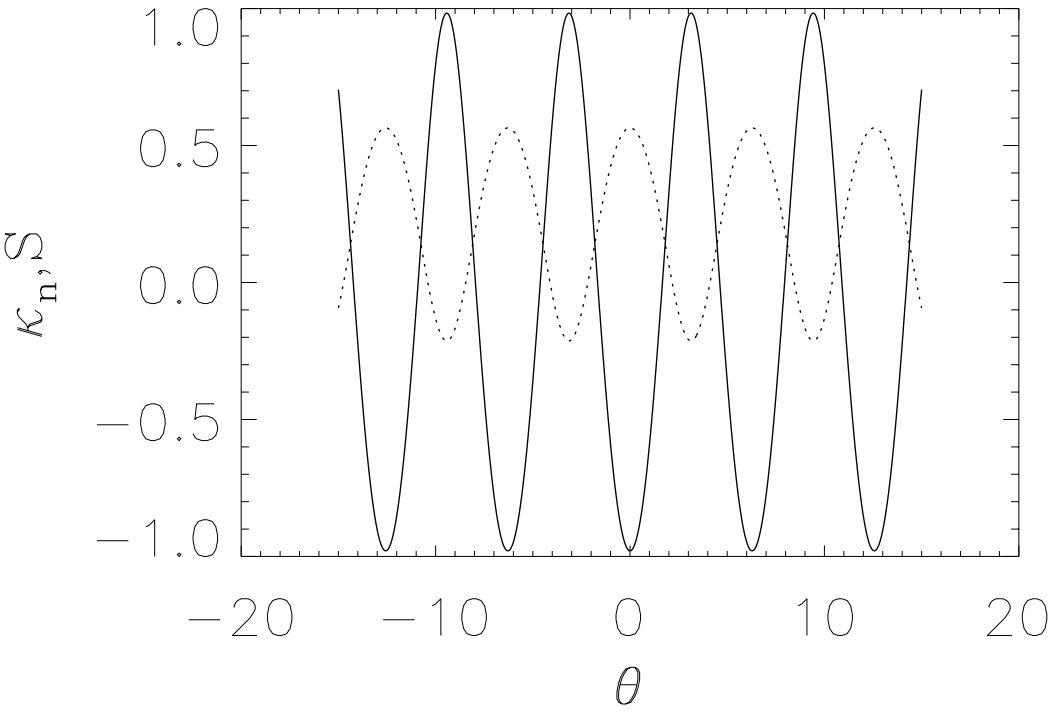

Fig. 12. Normal magnetic curvature (plain line) and local magnetic shear (dotted line) along the magnetic field line for the parameters of $(\epsilon_t, \epsilon_h) = (0.1, 0.0)$.

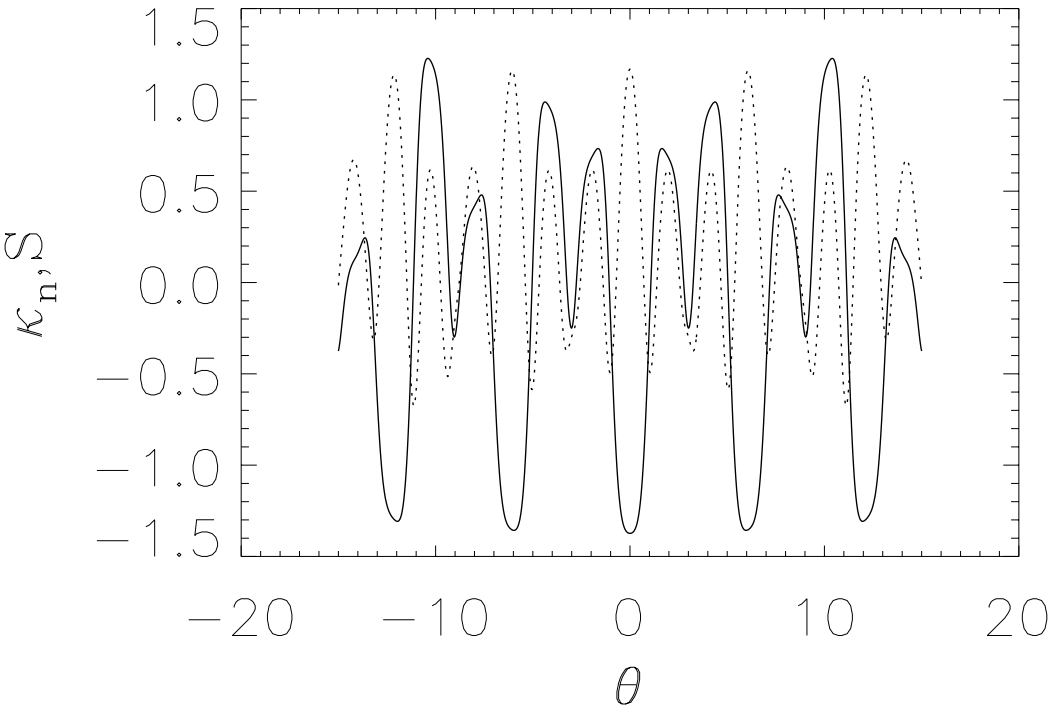

Fig. 13. Normal magnetic curvature (plain line) and local magnetic shear (dotted line) along the magnetic field line for the parameters of $(\epsilon_{\rm t}, \epsilon_{\rm h}) = (0.1, 0.1)$.

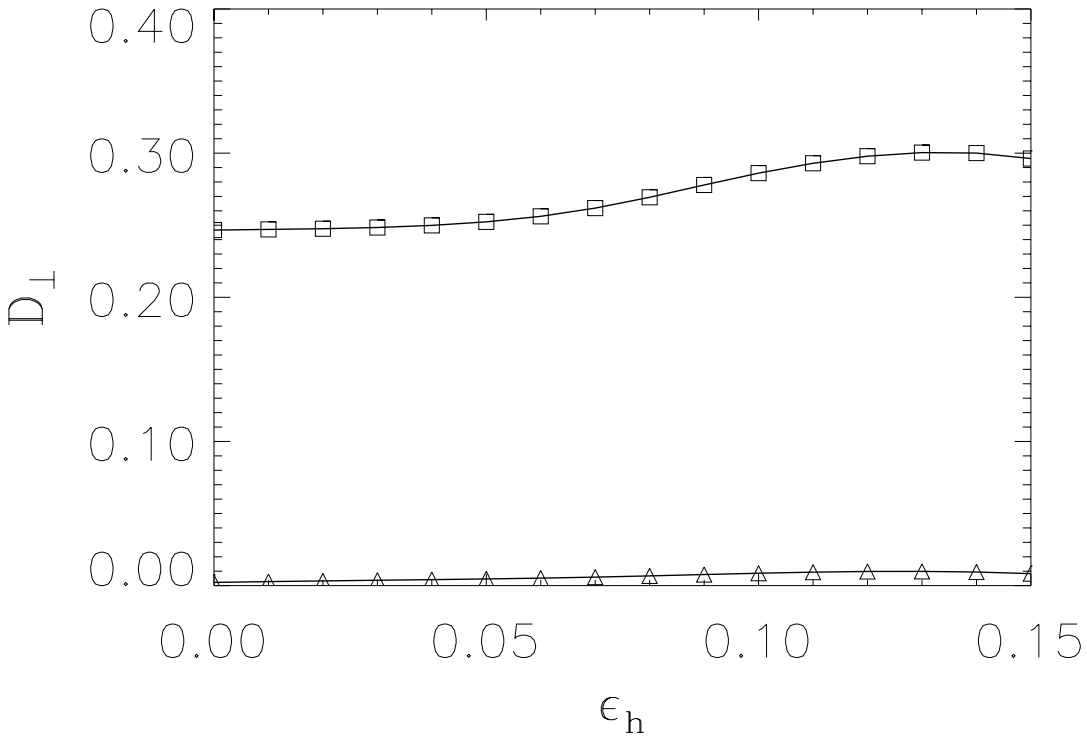

Fig. 14. Perpendicular diffusion coefficients $D_\perp^{(m)}$ (squares) and $D_\perp^{(fp)}$ (triangles) as a function of the helical parameter $\epsilon_{\rm h}$.

External Distribution

Plasma Research Laboratory, Australian National University, Australia

Professor I.R. Jones, Flinders University, Australia

Professor João Canalle, Instituto de Fisica DEQ/IF - UERJ, Brazil

Mr. Gerson O. Ludwig, Instituto Nacional de Pesquisas, Brazil

Dr. P.H. Sakanaka, Instituto Fisica, Brazil

The Librarian, Culham Laboratory, England

Mrs. S.A. Hutchinson, JET Library, England

Professor M.N. Bussac, Ecole Polytechnique, France

Librarian, Max-Planck-Institut für Plasmaphysik, Germany

Jolan Moldvai, Reports Library, Hungarian Academy of Sciences, Central Research Institute for Physics, Hungary

Dr. P. Kaw, Institute for Plasma Research, India

Ms. P.J. Pathak, Librarian, Institute for Plasma Research, India

Ms. Clelia De Palo, Associazione EURATOM-ENEA, Italy

Dr. G. Grosso, Instituto di Fisica del Plasma, Italy

Librarian, Naka Fusion Research Establishment, JAERI, Japan

Library, Laboratory for Complex Energy Processes, Institute for Advanced Study, Kyoto University, Japan

Research Information Center, National Institute for Fusion Science, Japan

Dr. O. Mitarai, Kyushu Tokai University, Japan

Dr. Jiangang Li, Institute of Plasma Physics, Chinese Academy of Sciences, People's Republic of China

Professor Yuping Huo, School of Physical Science and Technology, People's Republic of China

Library, Academia Sinica, Institute of Plasma Physics, People's Republic of China

Librarian, Institute of Physics, Chinese Academy of Sciences, People's Republic of China

Dr. S. Mirnov, TRINITI, Troitsk, Russian Federation, Russia

Dr. V.S. Strelkov, Kurchatov Institute, Russian Federation, Russia

Professor Peter Lukac, Katedra Fyziky Plazmy MFF UK, Mlynska dolina F-2, Komenskeho Univerzita, SK-842 15 Bratislava, Slovakia

Dr. G.S. Lee, Korea Basic Science Institute, South Korea

Institute for Plasma Research, University of Maryland, USA

Librarian, Fusion Energy Division, Oak Ridge National Laboratory, USA

Librarian, Institute of Fusion Studies, University of Texas, USA

Librarian, Magnetic Fusion Program, Lawrence Livermore National Laboratory, USA

Library, General Atomics, USA

Plasma Physics Group, Fusion Energy Research Program, University of California at San Diego, USA

Plasma Physics Library, Columbia University, USA

Alkesh Punjabi, Center for Fusion Research and Training, Hampton University, USA

Dr. W.M. Stacey, Fusion Research Center, Georgia Institute of Technology, USA

Dr. John Willis, U.S. Department of Energy, Office of Fusion Energy Sciences, USA

Mr. Paul H. Wright, Indianapolis, Indiana, USA

The Princeton Plasma Physics Laboratory is operated
by Princeton University under contract
with the U.S. Department of Energy.

Information Services
Princeton Plasma Physics Laboratory
P.O. Box 451
Princeton, NJ 08543

Phone: 609-243-2750
Fax: 609-243-2751
e-mail: pppl_info@pppl.gov
Internet Address: http://www.pppl.gov